AGU100 ADVANCING EARTH AND SPACE SCIENCE

Tectonics

RESEARCH ARTICLE
10.1029/2018TC005150

Key Points:
- First apatite fission track and apatite (U-Th-Sm)/He data of Thurston Island constrain thermal evolution since the Late Paleozoic
- Basin development occurred on Thurston Island during the Jurassic and Early Cretaceous
- Early to mid-Cretaceous convergence on Thurston Island was replaced at ~95 Ma by extension and continental breakup

Supporting Information:
- Supporting Information S1

Correspondence to:
M. Zundel,
zundel@uni-bremen.de

Citation:
Zundel, M., Spiegel, C., Mehling, A., Lisker, F., Hillenbrand, C.-D., Monien, P., & Klügel, A. (2019). Thurston Island (West Antarctica) between Gondwana subduction and continental separation: A multistage evolution revealed by apatite thermochronology. *Tectonics*, *38*, 878–897. https://doi.org/10.1029/2018TC005150

Received 28 MAY 2018
Accepted 24 JAN 2019
Accepted article online 30 JAN 2019
Published online 7 MAR 2019
Corrected 15 APR 2019

This article was corrected on 15 APR 2019. See the end of the full text for details.

Thurston Island (West Antarctica) Between Gondwana Subduction and Continental Separation: A Multistage Evolution Revealed by Apatite Thermochronology

Maximilian Zundel[1], Cornelia Spiegel[1], André Mehling[1], Frank Lisker[1], Claus-Dieter Hillenbrand[2], Patrick Monien[3], and Andreas Klügel[3]

[1]Department of Geosciences, Geodynamics of Polar Regions, University of Bremen, Bremen, Germany, [2]British Antarctic Survey, Cambridge, UK, [3]Department of Geosciences, Petrology of the Ocean Crust, University of Bremen, Bremen, Germany

Abstract The first low-temperature thermochronological data from Thurston Island, West Antarctica, provide insights into the poorly constrained thermotectonic evolution of the paleo-Pacific margin of Gondwana since the Late Paleozoic. Here we present the first apatite fission track and apatite (U-Th-Sm)/He data from Carboniferous to mid-Cretaceous (meta-) igneous rocks from the Thurston Island area. Thermal history modeling of apatite fission track dates of 145–92 Ma and apatite (U-Th-Sm)/He dates of 112–71 Ma, in combination with kinematic indicators, geological information, and thermobarometrical measurements, indicate a complex thermal history with at least six episodes of cooling and reheating. Thermal history models are interpreted to reflect Late Paleozoic to Early Mesozoic tectonic uplift of pre-Jurassic arc sequences, prior to the formation of an extensional Jurassic-Early Cretaceous back-arc basin up to 4.5 km deep, which was deepened during intrusion and rapid exhumation of rocks of the Late Jurassic granite suite. Overall Early to mid-Cretaceous exhumation and basin inversion coincided with an episode of intensive magmatism and crustal thickening and was followed by exhumation during formation of the Zealandia-West Antarctica rift and continental breakup. Final exhumation since the Oligocene was likely triggered by activity of the West Antarctic rift system and by glacial erosion.

1. Introduction

West Antarctica was formerly situated along the paleo-Pacific margin of Gondwana and comprises four major crustal blocks, including the Thurston Island block (TIB), the Antarctic Peninsula, the Ellsworth-Whitmore Mountains block, and the Marie Byrd Land block (Figure 1; Dalziel & Elliot, 1982). The latter block possibly comprised two provinces, eastern and western Marie Byrd Land (Figure 1a; Pankhurst et al., 1998). During long-lasting Paleozoic and Mesozoic subduction, accretion of the four crustal blocks against the East Antarctic craton formed the paleo-Pacific margin of Gondwana. Extension since the Jurassic led to Gondwana breakup and the separation of crustal blocks. Breakup was associated with mid-Cretaceous rifting within the Antarctic continent along the West Antarctic rift system (WARS; Siddoway, 2008) and along the Zealandia-West Antarctica rift (including, among others, Chatham Rise and Campbell Plateau; Figures 1b and 1c). The Zealandia continent was eventually separated from West Antarctica by seafloor spreading along the Pacific Antarctic Ridge prior to 83 Ma (Figure 1c; Eagles et al., 2004; Larter et al., 2002).

The current knowledge about the evolution of the paleo-Pacific margin is still fragmentary. This is because >98% of West Antarctica is covered by ice, while most Gondwana-related signatures in Zealandia are overprinted by younger processes (e.g., Mortimer et al., 2016). The main open questions include the following: (i) the pre-extensional (generally pre-mid-Cretaceous) evolution of the paleo-Pacific margin; (ii) the timing and extent of mid-Cretaceous extension related to the Zealandia-West Antarctica rift and the WARS prior to oceanic crust formation; and (iii) post breakup processes and landscape evolution of West Antarctica, as it provides crucial information for the onset and development of continental glaciation.

Thurston Island, which lies on the TIB, is situated close to the former triple junction of the Paleozoic-Mesozoic subduction margin and the newly developing Pacific-Antarctic-Ridge and may thus hold important information for understanding the subduction and extension history of East Gondwana (Figure 1c). Thurston Island forms a ~250-km-long and 50–100-km-wide island separating the

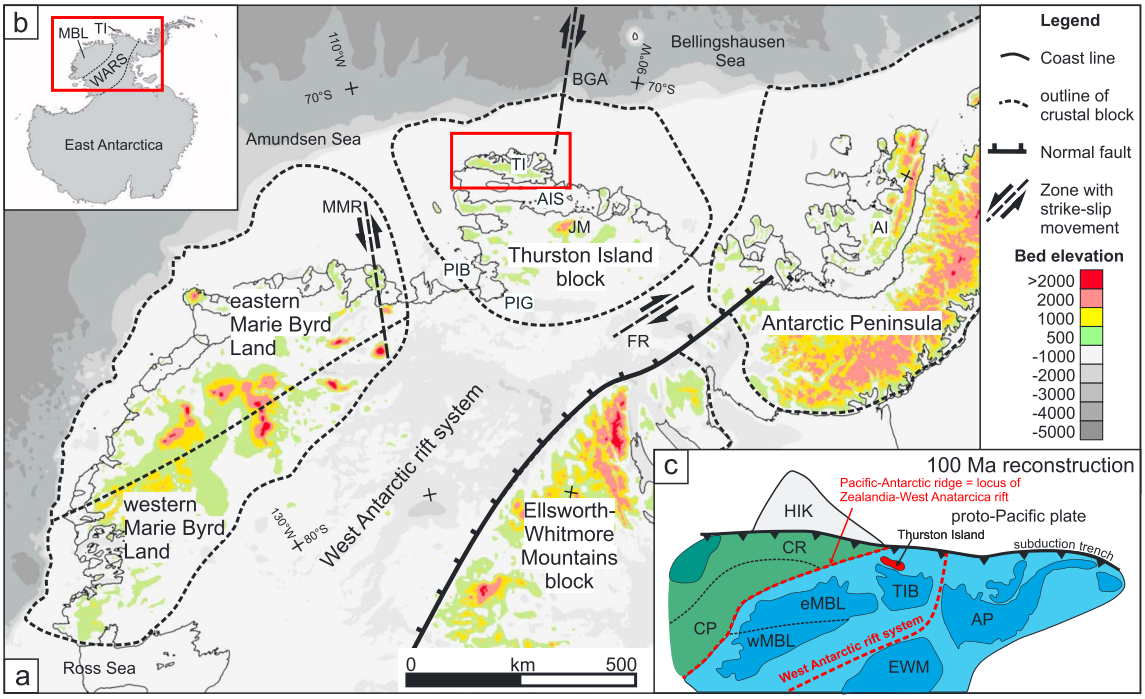

Figure 1. (a) Map showing the study area in the Thurston Island area (red box) in West Antarctica, which comprises four crustal blocks (outlined by dashed line): (i) Thurston Island block, (ii) Marie Byrd Land, (iii) Antarctic Peninsula, and (iv) Ellsworth-Whitmore Mountains block. The crustal block of Marie Byrd Land encompasses a western and an eastern realm (Pankhurst et al., 1998). Map also depicts ice-free topography (Bedmap2: Fretwell et al., 2013) and tectonic structures (LeMasurier, 2008; Müller et al., 2007; Spiegel et al., 2016). (b) Location of Figure 1a on the Antarctic continent. (c) Paleogeographic situation of the paleo-Pacific margin and tectonic plates of Antarctica (blue), Zealandia (green), and the Hikurangi Plateau (light grey) at ~100 Ma (Gohl et al., 2013). Thurston Island is highlighted in red. Present-day continental shelves are shown in light colors; emergent land is dark colored. Abbreviations: AI = Alexander Island, AIS = Abbot Ice Shelf, AP = Antarctic Peninsula, BGA = Bellingshausen Gravity Anomaly, CP = Campbell Plateau, CR = Chatham Rise; eMBL = eastern Marie Byrd Land, EWM = Ellsworth-Whitmore Mountains block, FR = Ferrigno Rift, HIK = Hikurangi Plateau, JM = Jones Mountains, MMR = Mount Murphy Rift, PIB = Pine Island Bay, PIG = Pine Island Glacier, TI = Thurston Island, TIB = Thurston Island block, WANT = West Antarctica, WARS = West Antarctic rift system, wMBL = western Marie Byrd Land.

Amundsen Sea and the Bellingshausen Sea at the West Antarctic continental margin (Figure 1a). The remote location with mostly unstable weather conditions, a vast ice cover, and very limited rock exposure has only allowed for very few geoscientific studies on Thurston Island (e.g., Grunow et al., 1991; Leat et al., 1993; Pankhurst et al., 1993; Riley et al., 2017; Storey et al., 1991). However, unlike Marie Byrd Land and Zealandia, where mid-Cretaceous crustal extension is constrained by exhumation of metamorphic core complexes, basin development, and extensive A-type magmatism (Bache et al., 2014; McFadden et al., 2015; Schwartz et al., 2016; Siddoway, 2008; Tulloch et al., 2009; Weaver et al., 1994), rift-related indications are scarce on the TIB. Consequently, the timing of extension has to be indirectly inferred. As continental breakup was associated with pronounced exhumation (e.g., Lindow et al., 2016), thermochronology provides an ideal tool to monitor and constrain the shallow crustal tectonic processes active at that time.

The aim of this study was therefore to reconstruct the thermotectonic evolution of Thurston Island since the Late Paleozoic on the basis of thermochronological and petrological data. Data were obtained from apatite fission track (AFT) and apatite (U-Th-Sm)/He (AHe) analyses, combined with hornblende-thermobarometry to estimate emplacement depths of intrusions. The results of thermal history modeling of AFT and AHe data were then interpreted using the input of thermobarometrical constraints to assemble a comprehensive geological evolution for the block.

The new data and thermal history models presented here extend the recently published thermochronological information from eastern Marie Byrd Land and Pine Island Bay (Figure 1a; Lindow et al., 2016; Spiegel et al., 2016) and establish a more comprehensive understanding of exhumation and erosion along the Pacific margin of West Antarctica. Further, the data provided here illuminate the complex tectonic evolution since

the Late Paleozoic along the paleo-Pacific margin of Gondwana and its transition from an active to passive margin setting.

2. Geological Setting

2.1. Geodynamic Evolution of the Thurston Island Block

The TIB was part of a terrane-assemblage forming the active paleo-Pacific margin of eastern Gondwana over large periods in the Paleozoic and Mesozoic (Figure 1c). During that time, West Antarctica and Zealandia were contiguous while the proto-Pacific plate was subducted beneath these crustal areas since at least the Devonian/Carboniferous (Pankhurst et al., 1998; Riley et al., 2017; Yakymchuk et al., 2015). Discontinuous subduction until the mid-Cretaceous led to the intrusion of calk-alkaline magmatic bodies that can be traced from West Antarctica to Zealandia and Australia (see Boger, 2011, and references therein). Subduction at the paleo-Pacific margin terminated in the mid-Cretaceous and gave way to crustal extension and continental rifting. The regional change from subduction to rifting has been related to the following: (i) entrance of the Pacific-Phoenix spreading center into the subduction zone (Luyendyk, 1995; Mukasa & Dalziel, 2000); (ii) the collision of the Hikurangi Plateau with the paleo-Pacific margin (Davy, 2014; Davy et al., 2008); or (iii) the activity of a mantle plume (Storey et al., 1999; Weaver et al., 1994). Since the mid-Cretaceous, crustal extension between East Antarctica and the crustal blocks of West Antarctica and Zealandia led to the opening of the WARS, south of the TIB, and to the Zealandia-West Antarctica rift and incipient opening of the South Pacific north of the TIB (Luyendyk et al., 2003; Siddoway, 2008). This situation caused extreme stretching on the Thurston Island and Marie Byrd Land crustal blocks as they experienced relatively synchronous, two-sided rifting. However, oceanic crust only evolved in the Zealandia-West Antarctica rift in the Late Cretaceous and caused the separation of Zealandia from West Antarctica between 90 and 83 Ma (Eagles et al., 2004; Larter et al., 2002). During the Late Cretaceous, the West Antarctic erosion surface and its equivalents in Zealandia formed at low elevations along the coast of West Antarctica and Zealandia, which beveled pre-mid-Cretaceous rocks (e.g., LeMasurier & Landis, 1996). During the Cenozoic, and mostly from the Eocene-Oligocene onward, the WARS experienced renewed activity in the Ross Sea area, in the Mount Murphy Rift west of the TIB, along the Bellingshausen Gravity Anomaly northeast of Thurston Island, and in the Ferrigno Rift southeast of the TIB (Figure 1a; Cande et al., 2000; Müller et al., 2007; Spiegel et al., 2016). This WARS activity was further associated with pronounced exhumation of the Transantarctic Mountains (Prenzel et al., 2013, 2014), alkaline volcanism in Marie Byrd Land and TIB, and uplift of the Marie Byrd Land dome, which elevated parts of the formerly low-lying West Antarctic erosion surface to altitudes >3,000 m (LeMasurier, 2008; LeMasurier & Rocchi, 2005). Apart from the volcanic activity in the Jones and Hudson Mountains (see Figure 2a for location) and some block faulting along the western margins of the TIB (Lindow et al., 2016), little Cenozoic tectonic activity was recognized for the TIB.

2.2. Exposed Rock Units on Thurston Island

Thurston Island and the adjacent mainland areas of the Thurston Island crustal block comprises a basement sequence of (meta-) igneous rocks, which record Carboniferous to Late Cretaceous subduction along the paleo-Pacific margin (Leat et al., 1993; Nelson & Cottle, 2018; Pankhurst et al., 1993; Riley et al., 2017). Based on geochronology, the basement rocks of Thurston Island comprise several lithological units, while virtually no geological contacts are exposed (Pankhurst et al., 1993; Figure 2):

1. The pre-Jurassic basement comprises Late Carboniferous granite and Permo-Triassic granite-gabbro intrusions. Late Carboniferous granite bodies intruded at 349 ± 2 Ma (U-Pb zircon; Riley et al., 2017) and were metamorphosed prior to 286 Ma to form ortho-gneisses (Pankhurst et al., 1993). The Permo-Triassic intrusions were emplaced between 286 ± 8 and 239 ± 4 Ma on Thurston Island and at 215–208 Ma in the Jones Mountains (K-Ar hornblende, U–Pb zircon; Pankhurst et al., 1993; Riley et al., 2017; Nelson & Cottle, 2018).
2. Jurassic volcanism is evidenced by basaltic to rhyolitic lavas and volcaniclastic rocks, which show a low-grade metamorphic overprint and are exposed in the central parts of Thurston Island. They are constrained to 182–181 Ma and are considered to correlate with the Chon Aike Province V1 event exposed in Patagonia and the Antarctic Peninsula (Riley et al., 2017). Although the lithological contact is not

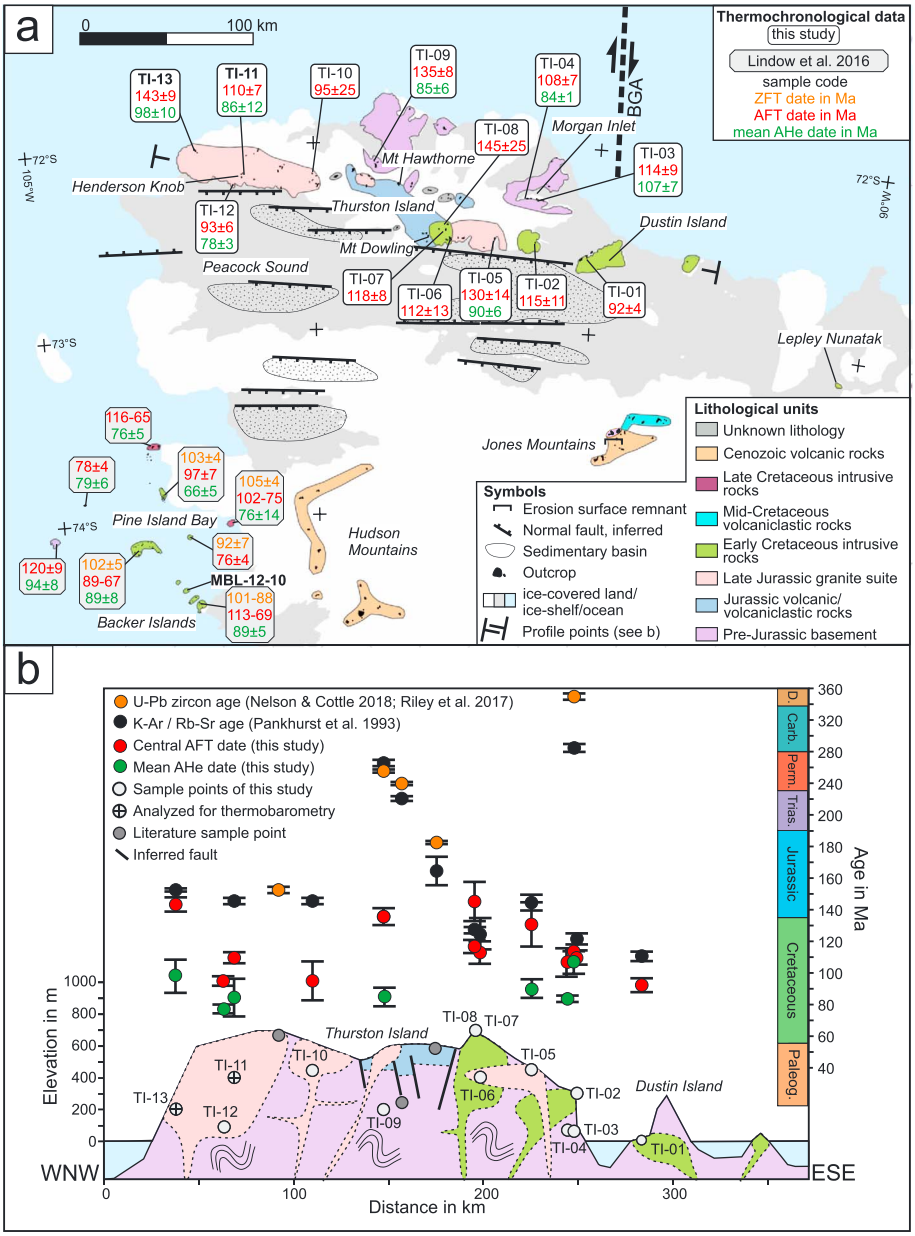

Figure 2. (a) Geological map of Thurston Island and the Pine Island Bay area together with low-temperature thermochronological data of this study and from the literature (Craddock et al., 1964; Lindow et al., 2016; Mukasa & Dalziel, 2000; Pankhurst et al., 1993, 1998; Riley et al., 2017; Storey et al., 1991; White & Craddock, 1987). Zircon (ZFT) and apatite fission track (AFT) dates are shown with 1σ error while mean apatite (U-Th-Sm)/He (AHe) dates are given with standard deviation. Bold sample codes highlight samples analyzed for thermobarometry. Contacts of the geological units are only rarely exposed so that spatial extent of the units is extrapolated. Sedimentary basins and inferred faults are adopted from Cochran et al. (2015) and are based on inversion of gravimetrical data. The dashed line northeast of the Morgan Inlet represents the southern continuation of the Bellingshausen Gravity Anomaly (BGA), which is considered to have accommodated dextral strike-slip movement (Müller et al., 2007). (b) Simplified WNW-ESE-profile across Thurston and Dustin Islands (for location of profile, see Figure 2a, vertical exaggeration ~85%). Sample points, partly projected onto the profile line, along with geochronological and thermochronological data are also shown. The distribution of lithological units is uncertain but is drawn schematically to demonstrate relative age relationships. For lithological units, see Figure 2a. Vertical bars refer to 1σ error.

exposed, the Jurassic volcanic and volcaniclastic rocks were presumably extruded and deposited, respectively, on a paleosurface on the pre-Jurassic basement, which crops out nearby at Mount Hawthorne (Figure 2a).

3. The Late Jurassic granite suite forms widespread granite-granodiorite intrusions in the western part of Thurston Island, with rare, more dioritic compositions (Leat et al., 1993). These intrusions are constrained by U-Pb zircon dating to 151 ± 2 Ma (Riley et al., 2017) and by Rb-Sr, K-Ar, and Ar-Ar techniques to 153–138 Ma (Pankhurst et al., 1993).
4. Early Cretaceous intrusive rocks comprise gabbro-diorite intrusions, yielding hornblende and biotite K-Ar and whole-rock Rb-Sr ages of 127–110 Ma, which are exposed in the eastern part of Thurston Island and on Dustin Island (Pankhurst et al., 1993).
5. Mid- to Late Cretaceous magmatism as a separate, identifiable magmatic episode is evidenced by silicic volcanic activity in the Jones Mountains. Felsic (dacite-rhyolite) lavas and tuffs and mafic-felsic dykes yielded ages ranging from 102 to 89 Ma (Rb-Sr whole rock: Pankhurst et al., 1993). This epdisode of magmatism is thought to be related to plate reorganization associated with subduction shut-off and onset of rifting on Thurston Island (Pankhurst et al., 1993).

The entire basement sequence (litholigcal units 1–5) was intruded by several mafic to felsic Cretaceous dykes that intruded prior to ~90 Ma (Leat et al., 1993). An undulatory, nearly horizontal erosion surface is exposed in the Jones Mountains, where it truncates pre-89 Ma rocks (Craddock et al., 1964; Pankhurst et al., 1993). This erosion surface is considered to have been connected to the Late Cretaceous West Antarctic erosion surface (LeMasurier, 2008; LeMasurier & Rocchi, 2005; Rocchi et al., 2006). Neogene volcanic rocks, with mainly basaltic compositions, prevail in the Hudson and Jones Mountains, while in the latter, they unconformably rest on the local erosion surface (Craddock et al., 1969; Hart et al., 1995).

2.3. Climatic Evolution of West Antarctica

The initial formation of large ice sheets in Antarctica supposedly commenced at the Eocene-Oligocene boundary, corresponding to a global temperature decrease (Barker et al., 2007; Zachos et al., 2001). Since the Oligocene, continental-scale ice sheets are considered to have continuously formed by expansion and coalescence of individual ice sheets to eventually form the West Antarctic Ice Sheet. The West Antarctic Ice Sheet, which nowadays covers most of the TIB and the adjacent Marie Byrd Land block, is believed to have formed during the (i) Late Eocene (Carter et al., 2017), (ii) Early Oligocene (Galeotti et al., 2016; Wilson et al., 2013), (iii) Early Miocene (Barker et al., 2007; Spiegel et al., 2016), or (iv) Middle to Late Miocene (Barker & Camerlenghi, 2002; Zachos et al., 2001). Today, several small glacial systems drain Thurston Island, while Peacock Sound is occupied by the Abbot Ice Shelf (Figure 1a). Unlike the rapidly thinning and retreating Pine Island Glacier, the Abbot Ice Shelf is affected by no significant or only very minor thinning (Figure 1a; Pritchard et al., 2012; Paolo et al., 2015).

3. Sampling and Methods

3.1. Sampling

Thirteen in situ bedrock samples used for this study were collected as part of a joint U.K.-U.S. West Antarctic tectonics project during the season 1984–1985 (samples stored at the British Antarctic Survey in Cambridge, UK) and during RV *Polarstern* expedition ANT-XXVI/3 in 2010. The samples were taken from 12 different locations on Thurston Island and from one location on Dustin Island (Table 1). Samples cover an elevation range from 5 to 700 m. Outcrop conditions, however, did not allow sampling of coherent elevation profiles. According to previously published intrusion ages, samples were subdivided into three groups (Table 1, Figure 2): (i) pre-Jurassic basement, including ortho-gneisses and diorites (TI-03, -04, -09); (ii) Late Jurassic granites, including granites, granodiorites, and diorites (TI-05, -10, -11, -12, -13); and (iii) Early Cretaceous intrusive rocks, comprising gabbroic rocks (TI-01, -02, -06, -07, -08).

3.2. AFT Thermochronology

AFT thermochronology is a temperature-sensitive radiogenic dating method based on the spontaneous decay of ^{238}U, causing lattice defects (fission tracks) within apatite crystals. Annealing of fission tracks occurs normally in the temperature interval of ~120–60 °C, which is why AFT thermochronology records geodynamic processes of the upper ~5 to 2 km of the continental crust. Fission tracks constantly accumulate over time, allowing for estimates of the duration, amount, and rate of rock cooling with respect to specific temperatures in the upper crust. Fission tracks completely anneal at temperatures >120 °C. At lower temperatures in the range of ~120 to 60 °C (referring to the Partial Annealing Zone [PAZ]), however, fission

Table 1
Sample Table Shows Central Apatite Fission Track (AFT) and Mean Apatite (U-Th-Sm)/He (AHe) Dates Obtained for This Study, in Addition to Other Published Geochronological Dates

Code	Location	Lat.	Long.	Elev. m	Sample lithology	Lithological unit	U-Pb[a] Ma	Rb-Sr[b] Ma	K-Ar,[b] Ar-Ar[b] Ma	AFT Ma	AHe Ma
TI-01	Dustin Island	−72.58	−95.12	5	Gabbro	Early Cretaceous intrusive rocks		111 ± 3 (bt)	110 ± 3 (bt)	92 ± 4	
TI-02	Harrison Nunatak	−72.52	−96.05	300	Gabbro	Early Cretaceous intrusive rocks		123 ± 20 (wr)	121 ± 6 (hb)	110 ± 7	
TI-03	Morgan Inlet	−72.29	−95.95	60	Ortho-gneiss	Pre-Jurassic basement	349 ± 2 (zr)	309 ± 5 (wr)	286 ± 8 (hb)	114 ± 9	107 ± 7
TI-04	Morgan Inlet	−72.29	−96.04	75	Ortho-gneiss	Pre-Jurassic basement	349 ± 2 (zr)	309 ± 5 (wr)	286 ± 8 (hb)	108 ± 7	84 ± 1
TI-05	Long Glacier	−72.51	−96.78	450	Granodiorite	Late Jurassic granite suite		144 ± 5 (wr)	142 ± 5 (hb)	130 ± 14	90 ± 6
TI-06	Shelton Head	−72.52	−97.33	450	Gabbro	Early Cretaceous intrusive rocks				112 ± 13	
TI-07	Belknap Nunatak	−72.44	−97.61	700	Gabbro	Early Cretaceous intrusive rocks		127 ± 4 (bt)	125 ± 3 (bt)	118 ± 8	
TI-08	Belknap Nunatak	−72.44	−97.63	700	Gabbro	Early Cretaceous intrusive rocks		125 ± 1 (bt)	125 ± 3 (bt)	145 ± 25	
TI-09	Guy Peaks	−72.11	−98.86	250	Diorite	Pre-Jurassic basement			265 ± 8 (hb)	135 ± 8	85 ± 6
TI-10	Mount Noxon	−72.17	−100.02	450	Granite	Late Jurassic granite suite	151 ± 2 (zr)	145 ± 2 (wr)		95 ± 25	
TI-11	Henderson Knob	−72.16	−101.22	400	Granodiorite	Late Jurassic granite suite	151 ± 2 (zr)	145 ± 2 (wr)	139 ± 4 (bt)	110 ± 13	86 ± 12
TI-12	Craft Glacier	−72.21	−101.39	80	Granite	Late Jurassic granite suite	151 ± 2 (zr)		139 ± 4 (bt)	93 ± 6	78 ± 2
TI-13	Landfall Peak	−72.02	−102.04	200	Diorite	Late Jurassic granite suite	151 ± 2 (zr)	153 ± 10 (wr)	152 ± 2 (bt)	143 ± 9	98 ± 10

Note. Indicated lithological units refer to those used in the text. bt = biotite, hb = hornblende, wr = whole rock, zr = zircon.
[a]Riley et al. (2017). [b]Pankhurst et al. (1993).

tracks tend to be partially preserved (Wagner et al., 1989). Fission track length shortening within the PAZ provides information on the style of cooling. Exact annealing temperatures depend on the chemical composition of apatite, which in turn is reflected by the etching rate. The mean diameter of fission track etch pits parallel to the crystallographic *c* axis is used as kinetic indicator (Dpar value: Donelick et al., 2005). The results of 256 dated apatites, track length, and Dpar measurements are shown in Table 2. Details on the laboratory procedures for AFT thermochronology are given in the supporting information (Text S1 and Figure S1).

3.3. Apatite (U-Th-Sm)/He Thermochronology

Apatite (U-Th-Sm)/He (AHe) thermochronology is based on the production of radiogenic ^{4}He as a daughter isotope of ^{238}U, ^{235}U, ^{232}Th, and ^{147}Sm. Diffusion in apatite at temperatures >85 °C leads to significant ^{4}He loss. ^{4}He is partially retained at temperatures between ~85 and 40 °C (He partial retention zone) and mostly accumulates within apatite at temperatures <40 °C (Wolf et al., 1998). Hence, AHe thermochronology records upper crustal dynamics at crustal depths of ~3 to 1 km. In addition to temperature-dependent diffusional loss, ^{4}He is lost by alpha-ejection along the outer ~20 μm rim of apatite grains, independent of temperature (Farley et al., 1996). To compensate for this effect, AHe raw dates in this study were corrected according to size and morphology of the analyzed grain, using the stopping distances of Ketcham et al. (2011). The results of AHe analyses are shown in Figure S2 and Table 3. For uncertainties and errors of AHe measurements, see Table S1 in the supporting information.

3.4. Thermal History Modeling

For thermal history modeling, we used the annealing algorithm of Ketcham et al. (2007a) for 5 M HNO_3 (Ketcham et al., 2007b) for AFT data and the He diffusion algorithm RDAAM of Flowers et al. (2009) for AHe data (Table S2). These algorithms are based on the experimentally determined fission track annealing and helium-diffusion behavior in apatite. The computer program HeFTy uses these equations to extrapolate the annealing and diffusion over geologic timescales (Ketcham, 2005). For this study, we used HeFTy version 1.8.3 to inversely produce continuous time-temperature paths (*t-T* paths), which were based on coupled AFT and AHe dates in combination with data on track length distributions and Dpar values. For modeling, track lengths were projected onto the *c* axis of corresponding apatite crystals (Ketcham et al., 2007a). For detailed model parameters and constraints, see the supporting information (Tables S2 and S3). Samples selected for modeling comprise at least 20 dated single apatite grains (fission track) and more than 70 confined track length measurements. Altogether, 10 AFT samples were modeled, of which six were supplemented by AHe data. For each sample, 100,000 paths were generated and tested. HeFTy compares modeled and observed thermochronological data and characterizes their match by a "goodness-of-fit" parameter (GOF). Resulting "acceptable" paths have a "goodness-of-fit" parameter of >0.05, and "good" paths have a "goodness-of-fit" parameter of >0.5. Good paths are in agreement with the sample data, whereas acceptable paths are not ruled out by the sample data. A comparison of measured and modeled data is shown in Table S4.

3.5. Hornblende Thermobarometry

Aluminum-in-hornblende barometry (Mutch et al., 2016) in combination with plagioclase-hornblende thermometry (Holland & Blundy, 1994) is used to calculate pressure and temperature during the crystallization of felsic intrusions. Thus, the composite hornblende thermobarometer allows for estimation of emplacement depths and associated geothermal gradients. These estimates may in turn improve the interpretation of thermochronological data, as they require assumptions on

Table 2
Results of Apatite Fission Track Analysis of the Thurston Island Area

Code	Location	Elevation m.a.s.l.	n	N_d	ρ_d 10^5 tracks/cm^2	N_s	ρ_s 10^5 tracks/cm^2	N_i	ρ_i 10^5 tracks/cm^2	$P(X)^2$ %	Central date Ma	U ppm	MTL ± 1σ µm	SD in µm	nMTL	Mean Dpar µm
TI-01	Dustin Island	5	20	14,639	18.77	747	0.108	2,233	0.323	62	92 ± 4	23	12.4 ± 0.2	2.0	100	2.04
TI-02	Harrison Nunatak	300	20	11,225	14.39	386	0.030	738	0.057	99	110 ± 7	5	14.1 ± 0.3	2.1	71	3.21
TI-03	Morgan Inlet	60	25	14,639	18.77	428	0.078	1,063	0.195	5	114 ± 9	14	13.0 ± 0.2	2.0	101	1.69
TI-04	Morgan Inlet	75	25	14,639	18.77	416	0.140	1,053	0.355	26	108 ± 7	25	13.0 ± 0.2	2.4	100	1.49
TI-05	Long Glacier	450	27	14,639	18.77	130	0.055	273	0.115	97	130 ± 14	8	12.9 ± 0.3	2.3	81	1.72
TI-06	Shelton Head	450	12	11,225	14.39	112	0.038	209	0.072	94	112 ± 13	7	14.2 ± 0.6	1.5	6	3.00
TI-07	Belknap Nunatak	700	20	13,249	16.99	334	0.090	699	0.188	100	118 ± 8	15	14.2 ± 0.2	1.4	78	3.23
TI-08	Belknap Nunatak	700	8	14,639	18.77	53	0.059	100	0.111	80	145 ± 25	8	13.0 ± 0.5	1.2	6	2.24
TI-09	Guy Peaks	250	22	14,639	18.77	530	0.120	1,074	0.243	65	135 ± 8	17	13.9 ± 0.1	1.4	100	2.23
TI-10	Mount Noxon	450	5	14,639	18.77	20	0.031	58	0.089	100	95 ± 25	6	13.3 ± 0.3	1.2	19	1.41
TI-11	Henderson Knob	400	20	14,639	18.77	113	0.057	281	0.141	96	110 ± 13	10	13.1 ± 0.2	1.6	100	1.57
TI-12	Craft Glacier	80	20	13,249	16.99	386	0.164	1,027	0.436	84	93 ± 6	34	12.4 ± 0.2	1.7	100	1.42
TI-13	Landfall Peak	200	32	14,639	18.77	486	0.033	930	0.098	100	143 ± 9	7	13.4 ± 0.2	2.0	106	1.78

Note. n = number of counted grains; N_d/ρ_d = number and density of tracks induced from dosimeter glass; N_s/ρ_s = number and density of spontaneous tracks; N_i/ρ_i = number and density of induced tracks; SD = standard deviation, U = uranium content; Zeta ζ = 294 ± 6 (M. Zundel), calculated for dosimeter glass IRMM540 (uranium = 13.9 ppm); MTL = mean track length (non-c-axis corrected values); nMTL = number of measured track lengths.

geothermal gradients to transform cooling rates into exhumation rates. The barometer is based on a linear relationship between pressure and the total aluminum content in hornblende. For accurate pressure determination, the mineral assemblage hornblende + plagioclase (An 15–80) + K-feldspar + biotite + titanite/ilmenite + quartz + magnetite is required (Mutch et al., 2016). The required assemblage was identified in thin-sections and in energy dispersive spectrometry in three samples, two of which were from Thurston Island, and another from Pine Island Bay (Figure 2b). Analyses were performed along straight grain boundaries, where amphibole and plagioclase are in direct contact (Figures S3a and S3b). Only fresh amphiboles were selected for analyses. We analyzed four to six pairs of hornblende-plagioclase rims per sample (Table S5). Electron microprobe analyzes were performed at the University of Bremen on a Cameca SX100 with four crystal wavelength dispersive spectrometers. A beam diameter of 5 µm, a beam current of 10 nA, and an accelerating voltage of 15 kV were used. The instrument was calibrated with Smithsonian standards (Jarosewich et al., 1980); the results of secondary standard analyses are shown in the supporting information (Table S6). Analyses were taken from the rims of euhedral grains and were averaged in Table 4, which also shows all temperature and pressure estimates in addition to inferred emplacement depths and geothermal gradients.

4. Results and Interpretation

4.1. Results of AFT Thermochronology

AFT dates from 11 samples from Thurston Island and Dustin Island range from 145 ± 25 to 92 ± 4 Ma (Figure 3a and Table 2). Mean track length (MTL) values vary between 12.4 and 14.2 µm, with standard deviations of 1.2–2.4 µm (Figure 3b). Mean Dpar values range from 1.4 to 1.8 µm for granitic to granodioritic samples, whereas dioritic to gabbroic samples show higher Dpar values of 2.0 to 3.2 µm (Figure 3c). All samples pass the χ^2 test at the 5% level, indicating that grains represent single-date populations (Table 2; Figure S1). AFT dates of most samples are younger than the corresponding crystallization ages (Table 1; Figure 2b; Pankhurst et al., 1993; Riley et al., 2017). Overlapping AFT dates and crystallization ages (considering 1σ error) exist at Harrison Nunatak (TI-02), Long Glacier (TI-05), Belknap Nunatak (TI-08), and Landfall Peak (TI-13). They indicate immediate post-intrusive cooling to temperatures <120 °C. However, TI-08 should be interpreted with caution, as the AFT date is based on only eight counted grains and thus of limited reliability. AFT dates show a positive correlation with sample elevation, with TI-09 and TI-13 shifted to older dates, indicating fault movement in between (Figure 3a). MTL values are positively correlated with sample elevations (Figure 3b). This trend is explained by a higher degree of track annealing due to a longer residence in the PAZ for samples from lower elevations. Track length distributions are generally negatively skewed, with some short track lengths of <10 µm. Short track lengths indicate protracted cooling within the temperature range of the PAZ. This feature is particularly pronounced for TI-01 and TI-12, which yielded 5–10% of tracks shorter than 10 µm and lower MTL of <13 µm. No apparent correlation of AFT dates with MTL is observed, which indicates that cooling was not caused by discrete rapid cooling events. Although Dpar values tend to increase with more mafic compositions of the sample's host rocks (Figure 3c), it is, however, not well understood which substitutions in apatite composition control Dpar in apatite (Donelick et al., 2005). A weak positive correlation of MTL with Dpar values (Figure 3c) could be explained by the fact that

Table 3
Results of Apatite (U-Th-Sm)/He Thermochronology From Thurston Island

Sample code Aliquot	Raw date Ma	Error Ma	Ft	^{4}He ncc	Mass µg	Sm ppm	Th ppm	U ppm	eU ppm	r_{sphere} µm	Corr. date Ma	Error Ma	Mean corr. date ± SD Ma
TI-03, Morgan Inlet, 60 m													
1	80	0.6	0.72	0.22	2	14.2	5.53	12.8	14	51	112	6	107 ± 7
2	81	0.6	0.75	0.43	5	14.5	3.42	8.72	10	63	108	5	
3	79	0.7	0.81	0.64	11	7.98	0.95	6.08	6	84	97	5	
4	85	0.8	0.77	0.61	6	15.7	4.56	9.24	10	69	111	6	
TI-04, Morgan Inlet, 75 m													
1	58	0.6	0.70	0.13	3	19.5	1.66	6.63	7	53	83	4	84 ± 1
2	*32*	*0.5*	*0.74*	*0.15*	*3*	*25.5*	*2.68*	*14.8*	*16*	*56*	*43*	*2*	
4	59	0.8	0.69	0.13	2	28.0	4.65	10.1	11	49	85	4	
5	63	0.6	0.76	0.74	5	24.9	10.3	15.3	18	60	83	4	
TI-05, Long Glacier, 450 m													
2	60	0.7	0.71	0.14	3	21.1	14.0	3.68	7	51	84	4	90 ± 6
3	60	0.8	0.61	0.16	2	40.0	23.0	9.86	15	41	98	5	
4	55	1.0	0.62	0.047	1	28.1	21.4	6.08	11	39	88	5	
5	58	0.8	0.65	0.11	1	46.0	23.8	10.7	17	43	88	5	
TI-09, Guy Peaks, 250 m													
2	63	0.6	0.77	0.74	4	17.2	42.6	16.4	27	64	82	4	85 ± 6
3	61	0.5	0.72	0.91	6	13.0	33.1	11.7	20	69	91	5	
5	59	0.9	0.66	0.19	1	19.9	48.8	13.9	25	43	89	5	
6	54	0.5	0.69	0.19	2	11.0	20.4	8.56	13	51	78	4	
TI-11, Henderson Knob, 400 m													
1	51	0.6	0.69	0.20	3	28.1	16.8	7.16	11	52	75	4	86 ± 12
2	56	0.5	0.61	0.22	1	21.5	60.1	19.9	34	42	87	4	
3	59	0.8	0.60	0.14	1	62.0	42.9	10.5	21	36	96	5	
4	66	1.4	0.65	0.36	1	107	80.0	21.2	41	43	101	5	
6	45	0.6	0.65	0.083	1	59.2	35.8	8.94	18	39	74	4	
TI-12, Craft Glacier, 80 m													
1	51	0.3	0.72	0.91	4	43.5	52.0	24.6	37	58	71	4	78 ± 2
2	59	0.2	0.71	1.76	3	62.4	108	47.8	74	55	83	4	
3	53	0.2	0.70	1.56	2	76.3	190	72.5	118	51	76	4	
4	51	0.3	0.63	0.45	1	64.0	99.7	63.5	87	40	81	4	
5	51	0.4	0.65	0.63	1	72.1	94.1	46.6	69	43	79	4	
TI-13, Landfall Peak, 200 m													
1	64	0.8	0.69	0.16	3	19.6	15.4	4.55	8	52	92	5	98 ± 10
2	74	1.1	0.69	0.19	3	22.2	15.4	5.01	9	52	107	6	
3	67	1.2	0.63	0.10	2	19.6	15.3	4.43	8	44	106	6	
4	54	0.6	0.62	0.092	1	19.3	21.3	6.07	11	42	88	4	

Note. Ft = α-ejection correction after Farley et al. (1996); ppm refers to ng/mg; r_{sphere} = equivalent sphere radius of measured crystal; SE = standard error; SD = standard deviation; eU = effective U content; all aliquots refer to single-grain measurements; figures in italics were not considered for mean dates.

the more mafic samples, which have a higher Dpar, belong to a younger lithological unit that cooled more rapidly through the PAZ.

4.2. Results of Apatite (U-Th-Sm)/He Thermochronology

Seven samples provided apatite crystals suitable for (U-Th-Sm)/He (AHe) dating. Derived single-grain AHe dates range from 112 ± 6 to 43 ± 2 Ma (Table 3). Intra-sample date dispersion is relatively high (up to 40 Myr), which is why mean AHe dates are reported with standard deviations. Aliquot #2 of TI-04 was regarded as an outlier and was not used for mean AHe date calculation and thermal history modeling. The mean AHe dates of all samples range from 107 ± 7 to 78 ± 2 Ma. Mean AHe dates of all samples are younger than the corresponding AFT dates, except for TI-03, where the AFT and the AHe dates are within 1σ error. AHe dates show no apparent spatial trend or correlation with sample elevation (Figure 2a; 3a). Effective uranium (eU) values range from 6 to 118 ppm (Table 3). Radii of analyzed apatite grains vary between 36 and 84 µm (Figure S2). Only weak correlations between grain date and eU and grain radii are

Table 4
Results of Hornblende Thermobarometry

Sample code		*n*	Plagioclase-hornblende temperature[a] (°C)	Al-in-hornblende pressure[b] (kbar)	Intrusion depth (km)	Geothermal gradient (°C/km)[c]
TI-11	**Mean**		**771 ± 38**	**2.7 ± 0.4**	**10 ± 1**	**76 ± 2**
	D2	5	766 ± 39	2.6 ± 0.4	10 ± 1	76 ± 3
	D3	4	768 ± 38	2.7 ± 0.4	10 ± 1	74 ± 1
	D4	4	784 ± 39	2.8 ± 0.4	11 ± 1	71 ± 1
	D6	5	767 ± 38	2.5 ± 0.4	9 ± 1	80 ± 5
TI-13	**Mean**		**887 ± 39**	**3.5 ± 0.6**	**13 ± 1**	**68 ± 3**
	D4	5	951 ± 38	3.5 ± 0.5	13 ± 1	71 ± 1
	D6	5	842 ± 38	3.5 ± 0.6	13 ± 1	64 ± 5
	D7	4	908 ± 38	4.0 ± 0.6	15 ± 1	59 ± 3
	D9	4	887 ± 38	3.8 ± 0.6	14 ± 1	61 ± 4
	D10	4	845 ± 40	2.6 ± 0.5	10 ± 0	85 ± 5
MBL-12-10	**Mean**		**676 ± 39**	**2.4 ± 0.3**	**9 ± 1**	**74 ± 6**
	D1	*3*	*585 ± 47*	*2.2 ± 0.4*	*8 ± 1*	*70 ± 6*
	D2	4	680 ± 38	2.5 ± 0.4	9 ± 0	70 ± 1
	D4	*5*	*608 ± 38*	*1.8 ± 0.3*	*7 ± 0*	*87 ± 4*
	D6	3	673 ± 39	2.4 ± 0.3	9 ± 1	78 ± 11
	D8	*5*	*648 ± 39*	*1.8 ± 0.3*	*7 ± 1*	*101 ± 11*
	D9	*3*	*605 ± 38*	*1.3 ± 0.3*	*5 ± 0*	*83 ± 5*

Note. Measurements in italics are excluded from mean value and further interpretations. D1, D2, ... = individual position of measurements; *n* = number of measurements; the uncertainties arise from the variation of individual measurements.
[a]Calculations after Holland and Blundy (1994). [b]Calculations after Mutch et al. (2016). [c]Based on overburden density of 2,700 kg/m^3, gravitational parameter of 9.83 m/s^2, and 20 °C surface temperature.

observed. TI-03, TI-05, and TI-11 reveal weak positive date-eU and inverse date-radius correlations (Figure S2). The former correlation indicates a potential influence of radiation damage on He retentivity of apatite, while the latter suggests enhanced He implantation from neighboring U-Th-Sm-rich minerals, which is enhanced at smaller grain-sizes due to a higher surface-to-volume ratio (Flowers et al., 2007; Spiegel et al., 2009). Despite these effects, TI-03 and TI-05 show overlapping single-grain dates (within 1σ error) with only one outlier each, suggesting rather rapid cooling (Flowers & Kelley, 2011). However, overdispersed AHe dates for TI-11 may indicate relatively slow cooling through the partial retention zone (Flowers et al., 2007; Flowers & Kelley, 2011). We exclude U and Th zonation as a reason for

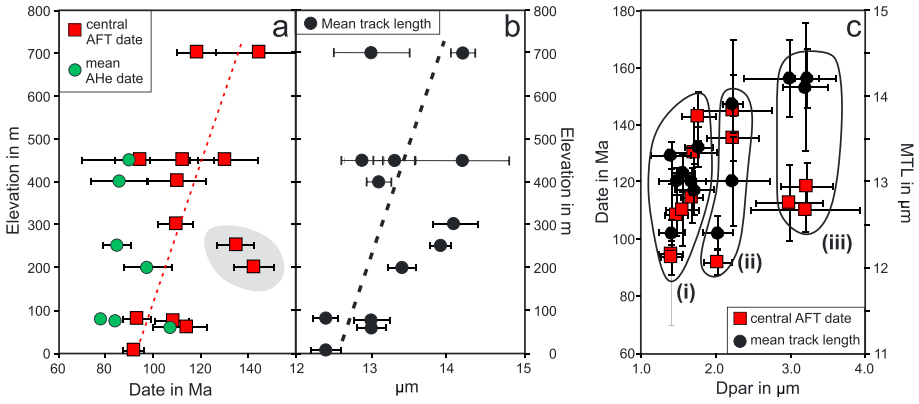

Figure 3. Thermochronological data plots. (a) Apatite fission track (AFT) and apatite (U-Th-Sm)/He (AHe) dates show a positive date-elevation trend (dashed line). TI-09 and TI-13 (grey area) are offset of this trend. (b) Mean track length (MTL) values show a positive trend (dashed line) with sample elevations. (c) Relation of mean track length (MTL) and apatite fission track ages with Dpar values outline three populations: (i) granites and granodiorites, (ii) diorites and gabbros, and (iii) gabbros.

overdispersion in this case because no track zonation was documented in the fission track mounts. TI-04 and TI-09 show overlapping single-grain dates within 1σ error and no apparent date-eU or date-radius correlations. TI-12 apatites yield high and variable eU values of 37–118 ppm together with an inverse correlation of AHe date and radius. This correlation and the broad span in eU can be explained by ^{4}He implantation from neighboring U-Th-Sm-rich minerals, as explained above (Spiegel et al., 2009). In the case of TI-12, this explanation is very likely because epidote and biotite occur together with apatite in interstitials between larger feldspar and quartz grains. Despite large eU variations, TI-12 shows overlapping single-grain AHe dates, which indicate rapid cooling (Flowers & Kelley, 2011). TI-13 shows overdispersed AHe dates without any date-eU or date-radius correlations. This finding may be explained by spatially variable eU concentrations, which correspond with frequently observed patchy distributions of greater track density in apatite grains of TI-13 in the fission track mounts. Such variability would lead to wrong corrections of AHe raw dates and thus undercorrected or overcorrected AHe dates (Flowers & Kelley, 2011). Following the recommendations of Flowers and Kelley (2011), AHe data from TI-13 were not considered for further interpretations. To account for radiation damage in our data set, thermal models were performed using the RDAAM apatite model (Flowers et al., 2009).

4.3. Results of Thermal History Modeling

Thermal history modeling is a powerful tool to constrain time-temperature paths from combined AFT and AHe data, covering a temperature range from ~40 to 120 °C. The thermal history modeling space was constrained by geochronometric and thermochronometric data and geological information. We placed the following temperature-time constraints: (1) geochronological dates (i.e., intrusion and cooling ages) and their corresponding closure temperatures >300 °C of the sample host rocks (Table S3); (2) the occurrence of Early Jurassic volcanic and volcaniclastic rocks at Mount Dowling, which imply an Early Jurassic paleosurface and thus (near-) surface temperatures of the underlying basement (Figure 2); (3) the predominance of Cretaceous AFT and AHe dates of the samples, which indicate reheating after Early Jurassic near-surface temperatures, motivating us to set another constraint at 170–80 Ma and 60–140 °C; and (4) the formation of the West Antarctic erosion surface, implying cooling during the Late Cretaceous. Because the exact timing and the formation process of the erosion surface in the study area are unknown, cooling was constrained to a wider interval of 110–60 Ma and to temperatures of 0–80 °C. Finally, all models end at 0 Ma and 0 °C. Samples were inversely modeled. In six of the models, sample AHe data was included with mean AHe dates and corresponding standard deviations. Resulting thermal history inversions are shown for individual samples in Figure 4. A compilation of weighted mean paths and their interpretation is shown in Figures 5a–5g. Figure 5a shows the following six cooling and reheating episodes:

1. Cooling of ~4–6 °C/Myr of pre-Jurassic basement (TI-03, -04, -09) from >500 °C (K-Ar hornblende; Pankhurst et al., 1993) to ~70 °C between 286–265 and ~175 Ma.
2. Reheating of pre-Jurassic basement to 100–115 °C between ~175 and 135–125 Ma at rates of ~1.5–1.8 °C/Myr. This episode includes intrusion and subsequent rapid cooling of parts of the Late Jurassic granite suite (TI-05, -11, -13) to ~80 °C during ~150–125 Ma. Post-emplacement cooling rates of 12–22 °C/Myr were constrained from thermal models and intrusion ages (Table 1).
3. Between ~135 and 95 Ma, pre-Jurassic basement underwent moderate cooling (1–3 °C/Myr) from temperatures of 100–115 to 35–75 °C. During this episode, all samples of the Late Jurassic granite suite cooled to temperatures <80 °C. This episode also involved rapid cooling (~13–22 °C/Myr) of the Early Cretaceous intrusive rocks from temperatures >300 °C to 80–90 °C between 127 and 95 Ma.
4. Between ~95 and 60 Ma, most samples cooled to temperatures <40 °C, at variable rates of ~0.2–1.1 °C/Myr. TI-01 and TI-12 remained at ~60–80 °C.
5. Between ~60 and 35 Ma, all samples cooled relatively slowly (<1 °C/Myr) to near-surface temperatures, while TI-01 and TI-04 remained at temperatures >40 °C.
6. Final cooling of most samples to 0 Ma and 0 °C occurred at slow rates of <1 °C/Myr. However, TI-01 and TI-12 show more enhanced cooling, starting from ~30 Ma and ~40 °C at rates of >1 °C/Myr.

4.4. Results From Hornblende Thermobarometry

Estimation of absolute exhumation in the study area requires constraints on intrusion depths of the host rocks of samples. Since Thurston Island was subject to major intrusive activity in the Mesozoic, it is

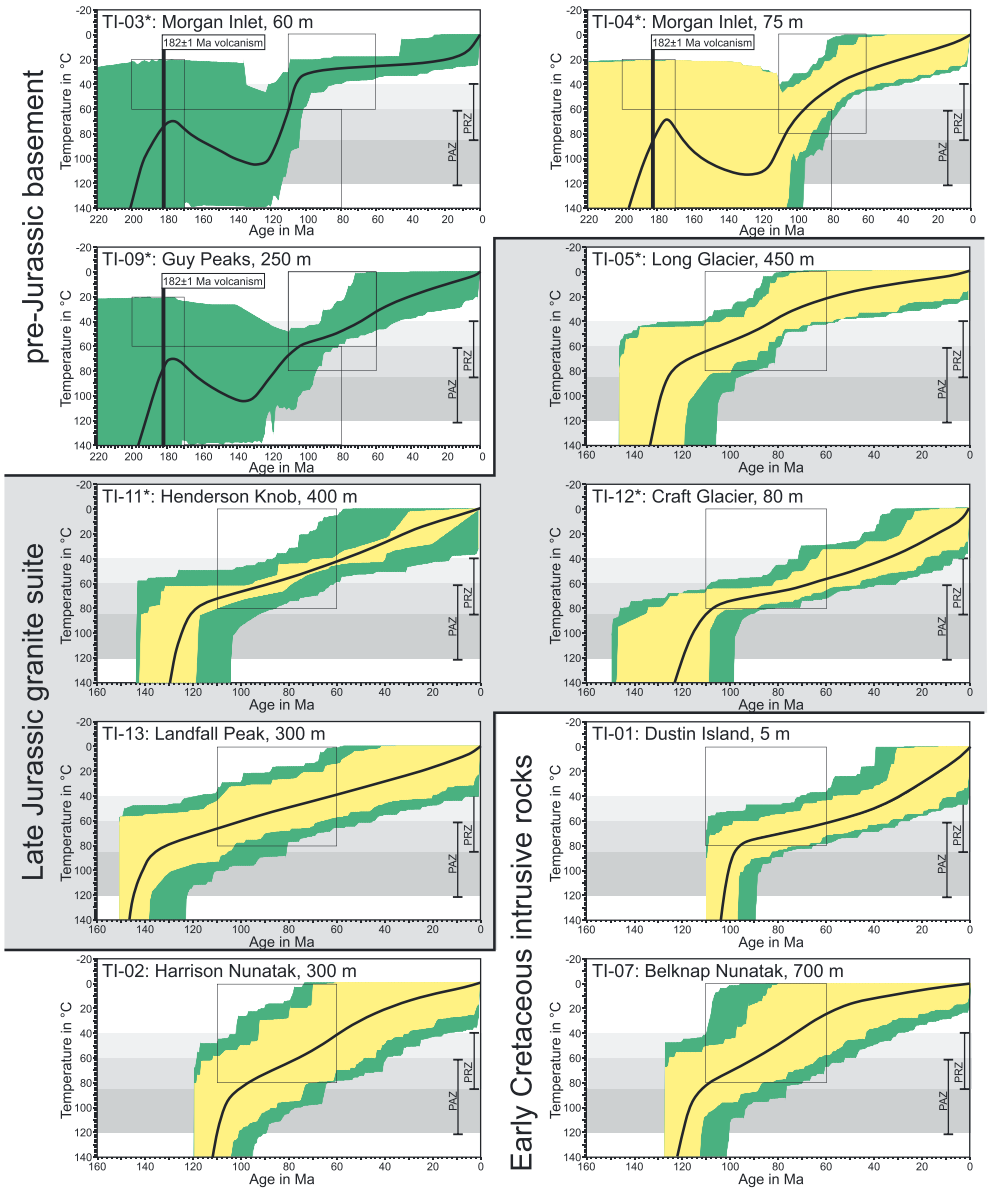

Figure 4. Results from HeFTy inverse modeling for the individual samples based on AFT data (AFT dates, track length distribution, and kinetic parameters). Models marked with an asterisk also include AHe data. Green and yellow areas indicate paths with a GOF of >0.05 and >0.5, respectively. Black curves represent weighted mean paths of the individual samples. Gray areas show the temperature ranges of the Partial Annealing Zone (PAZ) and Partial Retention Zone (PRZ). In these temperature ranges, the modeling results are most reliable for the applied thermochronometers. Volcanism at 182 ± 1 Ma is constrained by U-Pb zircon ages of volcanic and volcaniclastic rocks at Mount Dowling (Riley et al., 2017). These rocks suggest low temperatures of the adjacent pre-Jurassic basement. Black boxes mark the time-temperature constraints used for modeling. Models are based on Monte Carlo inversion and 100,000 randomly generated *t*–*T* paths.

essential to constrain geothermal gradients to transform cooling into exhumation. Therefore, intrusive rocks from Thurston Island and the Pine Island Bay area were analyzed for their emplacement depths and corresponding geothermal gradients. For hornblende thermobarometry, we analyzed a granodiorite and a diorite sample (TI-11 and TI-13) from the Late Jurassic granite suite on Thurston Island. Because samples from the Early Cretaceous intrusive rocks on Thurston Island did not match the required mineral assemblage for hornblende thermobarometry, we analyzed an Early Cretaceous hornblende-bearing granite (MBL-12-10) from the adjacent Pine Island Bay area instead (Figure 2a).

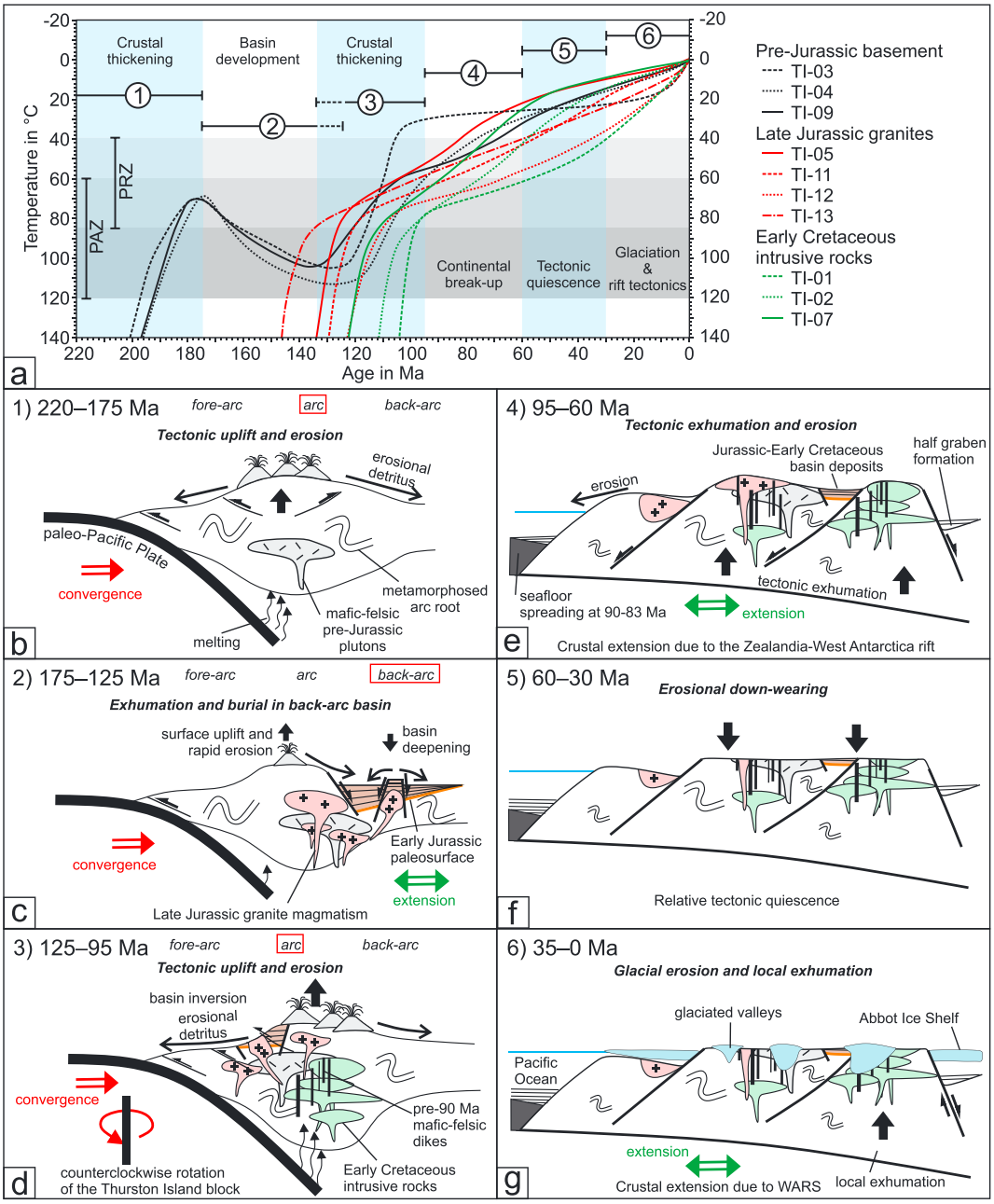

Figure 5. Compilation and interpretation of cooling paths. (a) Compilation of weighted mean paths of the Thurston Island area (taken from Figure 4), with six discerned cooling and heating episodes and their interpretation regarding the thermotectonic evolution. Gray areas show the temperature ranges of the Partial Annealing Zone (PAZ) and Partial Retention Zone (PRZ). Interpretation of the individual cooling and heating episodes is illustrated in panels (b) to (g). The location of Thurston Island in panels (b)–(d) is indicated by the red box. (b) Tectonic uplift and erosion caused exhumation of arc-related plutonic and metamorphic rocks within the convergent Late Paleozoic-Early Mesozoic active margin. (c) Intrusion of Late Jurassic granite suite caused surface uplift and rapid unroofing/erosion while a back-arc basin deepened. Note that rotation of the Thurston Island block (Grunow et al., 1991) probably occurred between panels (c) and (d). (d) Intensive Early Cretaceous magmatism and crustal thickening within the arc led to tectonic uplift and rapid exhumation on Thurston Island. (e) Crustal extension along the Zealandia-West Antarctica rift led to seafloor spreading and continental breakup during the Late Cretaceous. (f) Tectonic activity ceased after 60 Ma, followed by the successive erosional down-wearing of the basement. (g) Onset of glaciation was associated with surface modification while tectonic activity of the WARS caused local exhumation. Note that panels are not drawn to scale. Panels (d)–(g) are drawn roughly from north to south.

Chemical compositions of analyzed amphibole and plagioclase rims are shown in Table S5. Analyzed amphiboles show a composition of tschermakite, ferro-hornblende, and magnesio-hornblende (Figure S3c). Albite-rich plagioclase ($Ab_{65–79}$) occurs in TI-11 and MBL-12-10, while TI-13 comprises intermediate plagioclase ($Ab_{44–55}$). All temperature and pressure estimates are reported in Table 4. Mean calculated pressures range from 2.4 ± 0.4 to 3.5 ± 0.6 kbar, corresponding to emplacement depths of ~9–13 km. Four measurements of MBL-12-10 give pressures lower than the experimental calibration of the Al-in-hornblende barometer (2.5 kbar: Schmidt, 1992), and the hornblende-plagioclase thermometry for these measurements give temperatures below the H_2O-saturated solidus (Figure S3d; Mutch et al., 2016). Therefore, these results are unlikely to provide accurate hyper solidus pressure estimates. The remaining measurements give magmatic temperatures and consistent pressures for the individual samples. Granodioritic sample TI-11 from Henderson Knob (Figure 2a) yields intrusion depths of 10 ± 1 km and a geothermal gradient of 76 ± 2 °C/km (Table 4). This geothermal gradient refers to the interval ~150–140 Ma as constrained by U-Pb zircon and K-Ar biotite ages (Table 1). TI-13 from Landfall Peak shows deeper intrusion depths of 13 ± 1 km and a geothermal gradient of 68 ± 3 °C/km at ~150 Ma (Table 4). MBL-12-10 from the Backer Islands in Pine Island Bay gives intrusion depths of 9 ± 1 km and a geothermal gradient of 74 ± 6 °C/km.

5. Discussion

5.1. Late Paleozoic-Early Mesozoic Exhumation

Although the exact geographical position of the TIB during the Late Paleozoic-Early Mesozoic is still ambiguous (see Grunow et al., 1991; Riley et al., 2017; Veevers, 2012), there is consensus on an active margin setting at that time (Leat et al., 1993; Pankhurst et al., 1993). Such a setting was most likely associated with a high geothermal gradient of ~60–80 °C/km as indicated by our thermobarometrical analyses and supported by examples of the Andean magmatic arc (e.g., Bernet et al., 2016). Consequently, thermal history models together with high-temperature thermochronology and geochronology (Table 1) suggest Late Paleozoic-Early Mesozoic cooling of Thurston Island until the pre-Jurassic basement was exhumed to very shallow crustal depths of <1.2 km. This exhumation episode was most likely caused by erosion of pronounced topographic relief produced by convergence-driven crustal thickening and tectonic uplift (i.e., folding and thrusting) at the active continental margin (Figure 5b). Intensive erosion during this episode would have generated sedimentary detritus, which likely was deposited in contemporaneous Permo-Triassic fore-arc basins. Such basins were opening in the Antarctic Peninsula region (Millar et al., 2002, and references therein) and possibly on the Chatham Rise, where schists from the Chatham Islands were deposited prior to mid-Jurassic metamorphism (Adams & Robinson, 1977). Additionally, sediments could have been deposited in back-arc basin systems between the present Ross Sea and proto-Weddell Sea region during the Permian-Late Triassic Gondwanide Orogeny (Elliot, 1992; Elliot et al., 2016).

5.2. Jurassic to Early Cretaceous Basin Evolution

After cooling at shallow crustal levels in the Early Jurassic, our thermal history models record Early Jurassic-Early Cretaceous basement heating to temperatures of ~100–115 °C. This prolonged temperature increase, which caused a complete reset of AFT and AHe dates on Thurston Island, suggests burial of the pre-Jurassic basement in a previously unknown basin (Figure 5c). Basin development on Thurston Island was associated with deposition and extrusion of Early Jurassic bimodal volcanic and volcaniclastic rocks, presumably on a paleosurface that truncates the pre-Jurassic basement. Depending on the crustal depth of samples of the pre-Jurassic basement relative to the Early Jurassic paleosurface, a maximum basin infill of the Jurassic-Early Cretaceous basin of ~4.5–1.1 km existed at ~135–125 Ma, assuming geothermal gradients of 25–45 °C/km adopted from a Jurassic-Eocene basin in the Transantarctic Mountains (Prenzel et al., 2018). However, this inferred basin infill needs to be interpreted with caution, as we do not know the position of samples relative to the paleosurface. Nevertheless, basin infill must have been substantial, that is, >2 km, in order to cause a low-grade metamorphic overprint of the alleged basin deposits, which we assume are the Early Jurassic volcanic and volcaniclastic rocks reported by Pankhurst et al. (1993). The tectonic setting of the basin cannot be determined from our data alone and has to be inferred from the paleotectonic context. According to Riley et al. (2017), the TIB has rotated 180° since the Early Jurassic. An inferred Early Jurassic position of Thurston Island was therefore likely in a back-arc environment (Figure 6a). Other reconstructions, however, suggest a position of Thurston Island within or close to the fore-arc in the Jurassic (Elliot

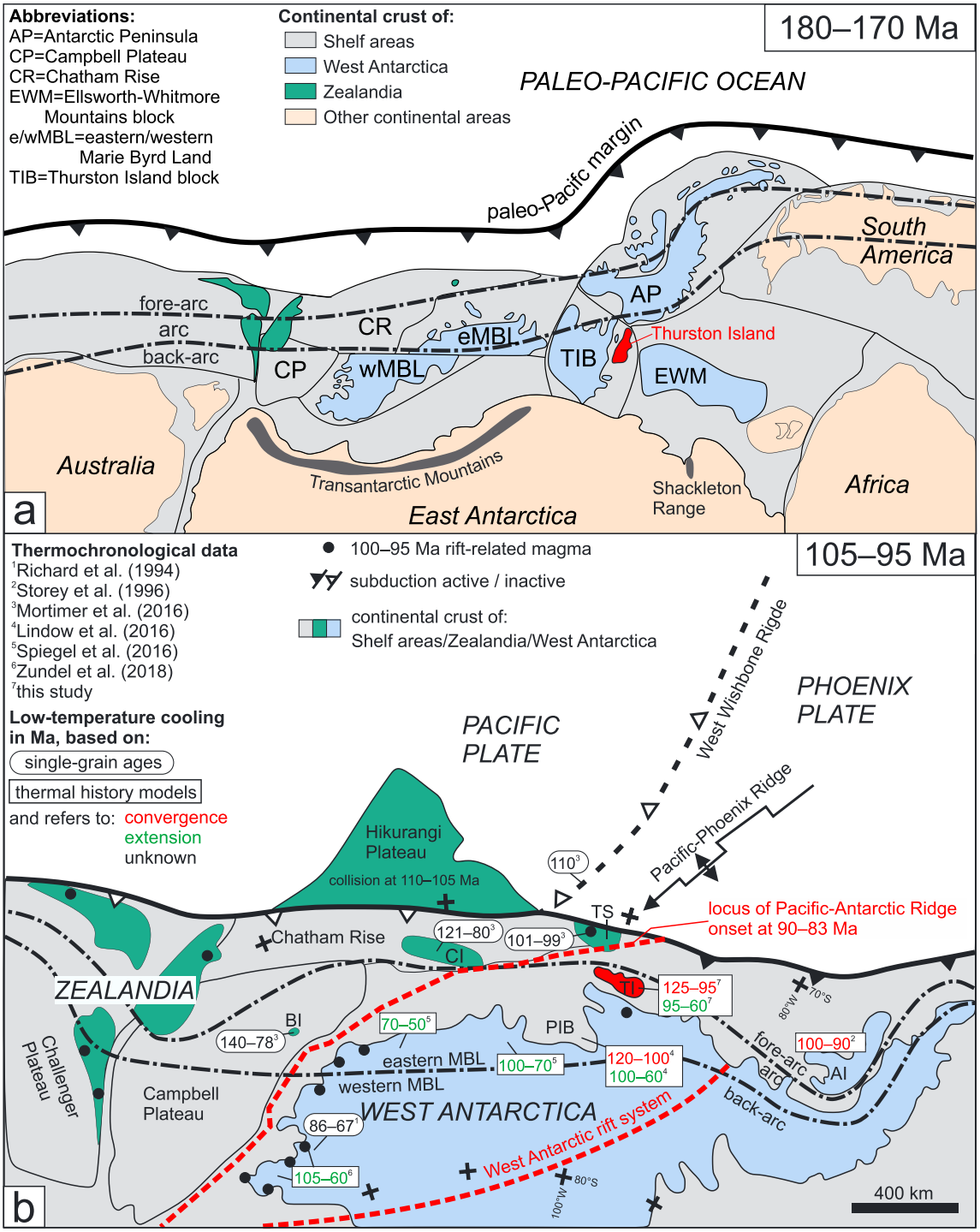

Figure 6. (a) Reconstruction of the active paleo-Pacific margin of Gondwana in the Early Jurassic (Elliot, 2013; Veevers, 2012). According to data of this study, Thurston Island (highlighted in red) likely occupied a back-arc position in the Early Jurassic. (b) Paleogeographic reconstruction of the paleo-Pacific margin of Gondwana for the mid-Cretaceous focusing on Zealandia and West Antarctica (Mortimer et al., 2006; Veevers, 2012). Also shown are areas that underwent Cretaceous low-temperature cooling, based on zircon fission-track, zircon (U-Th-Sm)/He, apatite fission track, and apatite (U-Th-Sm)/He dates. Abbreviations: AI = Alexander Island, BI = Bounty Islands, CI = Chatham Islands, TS = Takahe Seamount, MBL = Marie Byrd Land, PIB = Pine Island Bay, TI = Thurston Island.

et al., 2016; Grunow et al., 1991; Veevers, 2012). Although we cannot completely rule out an intra-arc or fore-arc basin setting, we favor the Riley et al. (2017) reconstruction, which includes the correlation of outcrop geology. Hence, the development of a Jurassic-Early Cretaceous back-arc basin on Thurston Island could

be tentatively explained by rollback of the subducted slab. Rollback is supported by the recognition of a relatively small accretionary prism between the former subduction trench and the magmatic arc (Figure 6a). Jurassic-Early Cretaceous back-arc extension occurred apparently contemporaneously with basin development in the Transantarctic Mountains (Lisker & Läufer, 2013; Prenzel et al., 2018) and in the Shackleton Range (Krohne et al., 2018), which is located to the southeast of the Weddell Sea embayment (Figure 6a). Therefore, Mesozoic intra-Gondwana extension sensu Lisker and Läufer (2013) may have also affected parts of the paleo-Pacific margin on the TIB.

Alternatively, reheating and resetting of the pre-Jurassic basement to temperatures of >120 °C may have been achieved by intrusions of the Late Jurassic granite suite at crustal depths of 10–13 km. According to Murray et al. (2018), intrusions of such midcrustal plutons are likely to reset low-temperature thermochronometers in the overlying country rocks if the ambient temperature is close to the closure temperature of the thermochronometers. However, because Early Jurassic volcaniclastic rocks rest on the pre-Jurassic basement, exhumation of pre-Jurassic basement rocks to crustal depths <1.2 km must have occurred by the Early Jurassic. This scenario requires subsequent burial to reset AFT and AHe thermochronometers at temperatures >120 °C, even for high geothermal gradients. In addition, Early Jurassic volcaniclastic sediments on Thurston Island exist and thus indicate that some sort of volcanic basin must have existed at that time. Therefore, in our view, the arguments for a Jurassic-Early Cretaceous basin on Thurston Island are more compelling than arguments for a thermal reset caused by Late Mesozoic plutonism.

5.3. Early Cretaceous Basin Inversion and Exhumation

Massive intrusions of the Late Jurassic granite suite on Thurston Island testify for renewed magmatic activity in the Late Jurassic, overlapping with Jurassic-Early Cretaceous back-arc basin evolution. Based on results of thermobarometry and weighted mean paths of thermal models, these magmatic bodies underwent diachronous rapid exhumation (~0.3–0.8 km/Myr) from crustal depths of ~10–13 km to ~1 km during the interval ~150–105 Ma. A scenario in which rocks of the Late Jurassic granite suite were rapidly exhumed while the Jurassic-Early Cretaceous back-arc basin deepened is shown in Figure 5c. In this scenario, parts of the Late Jurassic granite suite were exhumed along fault-bound blocks in the extending Jurassic-Early Cretaceous basin. Fault blocks formed high-relief domains, which were susceptible to rapid erosion (Figure 5c). Thus, combined exhumation by erosion and normal faulting led to rapid unroofing of the Late Jurassic granite suite while the generated erosional detritus was deposited in the deepening Jurassic-Early Cretaceous back-arc basin. Riley et al. (2017) already noted that Late Jurassic plutonism is relatively abundant on Thurston Island and in western Marie Byrd Land, whereas it is rare in eastern Marie Byrd Land and the Antarctic Peninsula. Thus, we suggest that a Late Jurassic magmatic episode was restricted to the back-arc environment of the paleo-Pacific margin, which is now exposed on Thurston Island and in western Marie Byrd Land (Figure 6a).

Our thermal history models suggest onset of renewed cooling of the pre-Jurassic basement at ~135–125 Ma. This exhumation episode was likely caused by rapid erosion of the Jurassic-Early Cretaceous basin deposits due to basin inversion. Early Cretaceous exhumation coincided with renewed magmatic activity in the Thurston Island area, that is, intrusive rocks with ages between 127 and 108 Ma were subject to subsequent rapid exhumation (~0.5 km/Myr) until ~95 Ma. Early to mid-Cretaceous magmatism was widespread along the entire paleo-Pacific margin and was related to terrane accretion and crustal thickening (Mukasa & Dalziel, 2000; Riley et al., 2017; Vaughan et al., 2012). Therefore, basin inversion and renewed magmatic activity strongly suggest that the Thurston Island area again underwent convergence since 135–125 Ma, superseding back-arc extension. This time probably marks the end of counterclockwise rotation of the TIB, which translated Thurston Island from an extensional back-arc environment to convergent arc tectonics, as already proposed by Grunow et al. (1991).

5.4. Late Cretaceous Exhumation

Intrusions with ages of 110–108 Ma on Dustin Island and at Lepley Nunatak are the youngest known subduction-related intrusions in the Thurston Island area (Figure 2a; Pankhurst et al., 1993; Riley et al., 2017). Slightly younger intrusions in the Pine Island Bay area constrain ongoing subduction activity on the TIB to 94 Ma (Mukasa & Dalziel, 2000). These 110–94 Ma old rocks probably intruded during a waning convergent regime. That regime was gradually replaced by extension, as indicated by rift-related magmatism

between 102 and 89 Ma on the TIB and at the Takahe Seamount, which is located at the eastern tip of Chatham Rise (Figure 6b; Kipf et al., 2012; Mortimer et al., 2006; Pankhurst et al., 1993), and onset of seafloor spreading at ~90–83 Ma between the TIB and the Chatham Rise (Eagles et al., 2004; Larter et al., 2002). In addition, high-standing topography produced by magmatic arc intrusions was largely reduced by ~60 Ma, as most samples cooled to temperatures <40 °C, indicating low denudation rates. Because of the eventual onset of extension leading to breakup and rapid reduction of mean surface elevation, we attribute cooling between 95 and 60 Ma on Thurston Island predominantly to variable tectonic denudation of ~1.9–0.2 km of crust (for geothermal gradients of 30–60 °C/km) due to normal faulting (Figure 5e). This interpretation is in agreement with contemporaneous tectonic denudation in the Pine Island Bay area (Lindow et al., 2016) and denudation by half graben formation in the Peacock Sound, which are assumed to have formed at ~90 Ma (Cochran et al., 2015). Because Thurston Island was located very close to the locus of the incipient Pacific-Antarctic Ridge, we suggest that tectonic denudation resulted from activity within the Zealandia-West Antarctic rift.

Cretaceous cooling was widespread along large portions of the paleo-Pacific margin (Figure 6b). Because of the rapid sequence of temporally and spatially overlapping events in the mid-Cretaceous to Late Cretaceous along this margin, cooling is difficult to attribute to a particular process. We interpret our thermochronological data of the Thurston Island area to record cooling between 135–125 and 95 Ma, resulting from convergent tectonics and associated crustal thickening. This time interval correlates with tectonic phases deduced from cooling signatures in the Pine Island Bay area (Lindow et al., 2016) and thus constrains subduction cessation on the TIB to ~95 Ma, which also coincided with deformation-related cooling on Alexander Island (Storey et al., 1996, Figure 6b). Early Cretaceous thermochronological dates from the Chatham Rise and Campbell Plateau indicate, but do not necessarily require, Early Cretaceous cooling, which was also likely associated with convergent subduction-related processes (Figure 6b). Our data indicate that convergence was replaced by extension at ~95 Ma in the Thurston Island area. This timing is roughly contemporaneous with the onset of low-temperature extension-related cooling in the Pine Island Bay area and in eastern Marie Byrd Land at ~100 Ma (Lindow et al., 2016; Spiegel et al., 2016). However, extension in western Marie Byrd Land was already established at ~105–100 Ma (Luyendyk et al., 2003; McFadden et al., 2015; Zundel, 2018) and thus 5–10 Ma earlier than 1,000 km to the east on the TIB. This trend is consistent with subduction shutoff from west to east along the paleo-Pacific margin due to oblique subduction (Figure 6b; e.g., Mukasa & Dalziel, 2000). The collision of the Hikurango Plateau at ~110–105 Ma with the margin (Davy, 2014) predates the onset of extension on the Thurston Island and Marie Byrd Land blocks by 5–10 Myr. If the Hikurangi collision had any effect on thermochronometers in more distant areas, then this effect was delayed by 5–10 Myr. With the current thermochronological data set we cannot rule out any of these scenarios as the main trigger mechanism for extension. However, we point out that both scenarios are compatible with the timing of low-temperature cooling on Thurston Island and probably both processes were active at the same time.

Cooling in West Antarctica during mid-Cretaceous to Late Cretaceous extension largely occurred between ~100 and 60 Ma (Figure 6b). The composite margin of Zealandia possibly underwent a similar evolution during the Late Cretaceous, as indicated by abundant bedrock single grain dates of apatite and zircon with corresponding dates (Figure 6b; Mortimer et al., 2016, and references therein). Late Cretaceous cooling in West Antarctica was, however, attributed to different processes. Spiegel et al. (2016) attributed rapid cooling at 100–60 Ma in eastern Marie Byrd Land to tectonic denudation and the activity along the WARS. Lindow et al. (2016) interpreted their data from the Pine Island Bay area as resulting from extension, following gravitational orogenic collapse. Conversely, Zundel (2018) found distinctive cooling episodes related to separate phases of the WARS and Zealandia-West Antarctica rift in western Marie Byrd Land. Apparently, cooling related to the Zealandia-West Antarctica rift was more pronounced in areas close to the breakup locus. In contrast, areas located more inland (i.e., Marie Byrd Land and the Pine Island Bay area) show cooling that was dominated by WARS activity.

5.5. Cenozoic Evolution

Between ~60 and 30 Ma, relatively rapid cooling in the Thurston Island area was followed by an episode of slow cooling, which we interpret as slow erosional down-wearing that led to the formation of the West Antarctic erosion surface (Figure 5f). Similar data were obtained for Cenozoic net denudation over an area of ~1,000 km in the Pine Island Bay area (Lindow et al., 2016) and in Marie Byrd Land (Spiegel et al., 2016;

Zundel, 2018). Such low denudation rates on a regional scale can be explained with a scenario of tectonic quiescence and a lack of significant relief. The age we conclude for the formation of the West Antarctic erosion surface is consistent with the timing proposed by Spiegel et al. (2016), but younger than the formation age between 85 and 75 Ma suggested by LeMasurier and Rocchi (2005).

Renewed cooling from up to 60 °C began at ~30 Ma and is related to a maximum denudation of 1.3 km, for geothermal gradients of 30–60 °C/km, until the present day. Within the sensitivity limits of thermochronological data, this denudation was only observed in TI-01 and TI-12 from western Thurston Island and Dustin Island, respectively (Figure 5a). Denudation during the Oligocene would be possible by enhanced valley erosion due to the onset of continental glaciation (Figure 5g; e.g., Wilson et al., 2013; Carter et al., 2017). Because Dustin Island lies exactly on trend to the south of the ~N-S striking deep crustal structure of the Bellingshausen Gravity Anomaly, post-Eocene denudation on Dustin Island could be alternatively explained by tectonic activity associated with this anomaly (Figure 2a; Gohl et al., 1997). Transcurrent and partly convergent tectonic activity along the Bellingshausen Gravity Anomaly is roughly constrained to the Late Cretaceous and to the mid-Cenozoic to late Cenozoic (Cunningham et al., 2002; Eagles et al., 2004; Gohl et al., 1997). Thus, post-Eocene denudation on Dustin Island can be explained by vertical block movements and enhanced erosion related to tectonic activity associated with this anomaly (Figure 5g). Hence, our data, together with findings of Gohl et al. (1997), identify tectonic activity along the Bellingshausen Gravity Anomaly to ~30–13 Ma. This interval agrees with interpretations of Müller et al. (2007) that a segment of the Cenozoic WARS exploited structures parallel to the Bellingshausen Gravity Anomaly.

6. Summary and Conclusions

Combined AFT and (U-Th-Sm)/He thermochronology data in addition to thermal history modeling applied to Paleozoic and Mesozoic (meta-) igneous rocks from Thurston Island and Dustin Island allow the following conclusions:

1. Samples from Thurston Island yield the oldest apatite fission track dates so far observed along the Pacific margin of West Antarctica. They preserve evidence for a complex rock cooling history with exhumation and burial episodes along the paleo-Pacific margin before, during, and after Gondwana breakup.
2. Thermal history models suggest that pre-Jurassic magmatic arc sequences on Thurston Island were subject to Late Paleozoic-Early Mesozoic exhumation. Exhumation was related to tectonic uplift and intensive erosion, resulting in the formation of an Early Jurassic paleosurface, which was re-exposed in the Late Cretaceous. This scenario implies that parts of the present-day landscape of Thurston Island formed already in the Jurassic and thus >80 Myr prior to the mid-Cretaceous landscape architecture of Marie Byrd Land.
3. Between the Early Jurassic and Early Cretaceous, Thurston Island was characterized by heating, which we interpret as burial resulting from back-arc basin development following widespread Early Jurassic volcanism. Basin development on Thurston Island shows striking similarities with the Mesozoic basins in the Shackleton Range (Krohne et al., 2018) and the Transantarctic Mountains (Lisker & Läufer, 2013). All these basins initiated by the Early Jurassic and thus indicate that Mesozoic intra-Gondwana extension extended over larger areas than previously thought.
4. All basement units in the Thurston Island area experienced cooling at ~135–125 Ma, corresponding with crustal thickening and rapid erosion of almost the complete Early Jurassic-Early Cretaceous basin deposits due to basin inversion until ~95 Ma. Subsequent relatively rapid exhumation during the Late Cretaceous was most likely related to extensional tectonics in response to activity of the Zealandia-West Antarctica rift at ~95–60 Ma. Onset of regional extension-related cooling in West Antarctica shows a tentative progression from western Marie Byrd Land (~105 Ma) to eastern Marie Byrd Land (~100 Ma) to the TIB (~95 Ma). We interpret this progression to be a response to the general subduction shut off along the Paleo-Pacific margin from west to east.
5. Well after continental breakup and between ~60 and 30 Ma, the Thurston Island area was characterized by low-denudation rates, which reflects tectonic quiescence, subdued topography, and the formation of the West Antarctic erosion surface close to sea level. This scenario suggests that only limited land areas were emergent and thus restricted the formation of continental ice sheets in Eocene-Oligocene times.

6. Based chiefly on the thermochronological data of one sample, we constrain tectonic activity of the WARS along structures running parallel to the Bellingshausen Gravity Anomaly to post-30 Ma. This interpretation implies that the TIB is internally dissected and may thus not be considered as a rigid block in Late Cenozoic times.

Acknowledgments
Constructive reviews of E. Enkelmann and R. Flowers as well as editorial handling of T. Schildgen are gratefully acknowledged. The authors thank A. Toltz (University of Bremen) and her team of student assistants for sample processing, and H. Blagbrough (British Antarctic Survey [BAS]) for help with providing the samples from the BAS rock collection. V. Kolb and C. Schott (both University of Bremen) are acknowledged for He measurements. S. Sopke (University of Bremen) is acknowledged for electron microprobe analysis. The authors are particularly grateful to P. Kamp (University of Waikato) for valuable suggestions and discussions. We thank captain U. Pahl of RV *Polarstern* and his crew, pilots from Heli International, scientific personnel and K. Gohl (chief scientist) for their support of rock sampling during expedition ANT-XXVI/3, and BAS and U.S. scientists and field personnel for collecting the rock samples stored at BAS. The German Science Foundation (DFG) is acknowledged for providing financial support, grant SP673/15-1, in the framework of the priority program SPP 1158 "Antarctic research with comparative investigations in Arctic ice areas." All data used are documented in the listed references, figures, tables, and supporting information.

References

Adams, C. J. D., & Robinson, P. (1977). Potassium-argon ages of schists from Chatham Island, New Zealand plateau, southwest Pacific. *New Zealand Journal of Geology and Geophysics*, *20*(2), 287–301. https://doi.org/10.1080/00288306.1977.10420708

Bache, F., Mortimer, N., Sutherland, R., Collot, J., Rouillard, P., Stagpoole, V., & Nicol, A. (2014). Seismic stratigraphic record of transition from Mesozoic subduction to continental breakup in the Zealandia sector of eastern Gondwana. *Gondwana Research*, *26*(3–4), 1060–1078. https://doi.org/10.1016/j.gr.2013.08.012

Barker, P. F., & Camerlenghi, A. (2002). Glacial history of the Antarctic Peninsula from Pacific margin sediments. In *Proceedings of the Ocean Drilling Program, scientific results* (Vol. 178, pp. 1–40). College Station, TX: Ocean Drilling Program.

Barker, P. F., Diekmann, B., & Escutia, C. (2007). Onset of Cenozoic Antarctic glaciation. *Deep Sea Research Part II: Topical Studies in Oceanography*, *54*(21–22), 2293–2307. https://doi.org/10.1016/j.dsr2.2007.07.027

Bernet, M., Urueña, C., Amaya, S., & Peña, M. L. (2016). New thermo and geochronological constraints on the Pliocene-Pleistocene eruption history of the Paipa-Iza volcanic complex, Eastern Cordillera, Colombia. *Journal of Volcanology and Geothermal Research*, *327*, 299–309. https://doi.org/10.1016/j.jvolgeores.2016.08.013

Boger, S. D. (2011). Antarctica—Before and after Gondwana. *Gondwana Research*, *19*(2), 335–371. https://doi.org/10.1016/j.gr.2010.09.003

Cande, S. C., Stock, J. M., Müller, R. D., & Ishihara, T. (2000). Cenozoic motion between east and west Antarctica. *Nature*, *404*(6774), 145–150. https://doi.org/10.1038/35004501

Carter, A., Riley, T. R., Hillenbrand, C. D., & Rittner, M. (2017). Widespread Antarctic glaciation during the late Eocene. *Earth and Planetary Science Letters*, *458*, 49–57. https://doi.org/10.1016/j.epsl.2016.10.045

Cochran, J. R., Tinto, K. J., & Bell, R. E. (2015). Abbot Ice Shelf, structure of the Amundsen Sea continental margin and the southern boundary of the Bellingshausen Plate seaward of West Antarctica. *Geochemistry, Geophysics, Geosystems*, *16*, 1421–1438. https://doi.org/10.1002/2014GC005570

Craddock, C., Bastien, T. W., & Rutford, R. H. (1964). Geology of the Jones Mountains area. *Antarctic Geology*, 171–187.

Craddock, C., White, C. M., & Rutford, R. H. (1969). Geology of Eights Coast. *Antarctic Journal of the United States*, *4*(4), 93.

Cunningham, A. P., Larter, R. D., Barker, P. F., Gohl, K., & Nitsche, F. O. (2002). Tectonic evolution of the Pacific margin of Antarctica 2. Structure of Late Cretaceous–early Tertiary plate boundaries in the Bellingshausen Sea from seismic reflection and gravity data. *Journal of Geophysical Research*, *107*(B12), 2346. https://doi.org/10.1029/2002JB001897

Dalziel, I. W., & Elliot, D. H. (1982). West Antarctica: Problem child of Gondwanaland. *Tectonics*, *1*(1), 3–19. https://doi.org/10.1029/TC001i001p00003

Davy, B. (2014). Rotation and offset of the Gondwana convergent margin in the New Zealand region following Cretaceous jamming of Hikurangi Plateau large igneous province subduction. *Tectonics*, *33*, 1577–1595. https://doi.org/10.1002/2014TC003629

Davy, B., Hoernle, K., & Werner, R. (2008). Hikurangi Plateau: Crustal structure, rifted formation, and Gondwana subduction history. *Geochemistry, Geophysics, Geosystems*, *9*, Q07004. https://doi.org/10.1029/2007GC001855

Donelick, R. A., O'Sullivan, P. B., & Ketcham, R. A. (2005). Apatite fission-track analysis. *Reviews in Mineralogy and Geochemistry*, *58*(1), 49–94. https://doi.org/10.2138/rmg.2005.58.3

Eagles, G., Gohl, K., & Larter, R. D. (2004). High-resolution animated tectonic reconstruction of the South Pacific and West Antarctic margin. *Geochemistry, Geophysics, Geosystems*, *5*, Q07004. https://doi.org/10.1029/2003GC000657

Elliot, D. H. (1992). Jurassic magmatism and tectonism associated with Gondwanaland break-up: An Antarctic perspective. *Geological Society, London, Special Publications*, *68*(1), 165–184. https://doi.org/10.1144/GSL.SP.1992.068.01.11

Elliot, D. H. (2013). The geological and tectonic evolution of the Transantarctic Mountains: A review. *Geological Society, London, Special Publications*, *381*, SP381–SP314. https://doi.org/10.1144/SP381.14

Elliot, D. H., Fanning, C. M., & Laudon, T. S. (2016). The Gondwana plate margin in the Weddell Sea sector: Zircon geochronology of upper Paleozoic (mainly Permian) strata from the Ellsworth Mountains and eastern Ellsworth Land, Antarctica. *Gondwana Research*, *29*(1), 234–247. https://doi.org/10.1016/j.gr.2014.12.001

Farley, K. A., Wolf, R. A., & Silver, L. T. (1996). The effects of long alpha-stopping distances on (U-Th)/He ages. *Geochimica et Cosmochimica Acta*, *60*(21), 4223–4229. https://doi.org/10.1016/S0016-7037(96)00193-7

Flowers, R. M., & Kelley, S. A. (2011). Interpreting data dispersion and "inverted" dates in apatite (U–Th)/He and fission-track datasets: An example from the US midcontinent. *Geochimica et Cosmochimica Acta*, *75*(18), 5169–5186. https://doi.org/10.1016/j.gca.2011.06.016

Flowers, R. M., Ketcham, R. A., Shuster, D. L., & Farley, K. A. (2009). Apatite (U–Th)/He thermochronometry using a radiation damage accumulation and annealing model. *Geochimica et Cosmochimica Acta*, *73*(8), 2347–2365. https://doi.org/10.1016/j.gca.2009.01.015

Flowers, R. M., Shuster, D. L., Wernicke, B. P., & Farley, K. A. (2007). Radiation damage control on apatite (U-Th)/He dates from the Grand Canyon region, Colorado Plateau. *Geology*, *35*(5), 447–450. https://doi.org/10.1130/G23471A.1

Fretwell, P., Pritchard, H. D., Vaughan, D. G., Bamber, J. L., Barrand, N. E., Bell, R., et al. (2013). Bedmap2: Improved ice bed, surface and thickness datasets for Antarctica. *The Cryosphere*, *7*(1), 375–393. https://doi.org/10.5194/tc-7-375-2013

Galeotti, S., DeConto, R., Naish, T., Stocchi, P., Florindo, F., Pagani, M., et al. (2016). Antarctic ice sheet variability across the Eocene-Oligocene boundary climate transition. *Science*, *352*(6281), 76–80. https://doi.org/10.1126/science.aab0669

Gohl, K., Nitsche, F., & Miller, H. (1997). Seismic and gravity data reveal Tertiary interplate subduction in the Bellingshausen Sea, southeast Pacific. *Geology*, *25*(4), 371–374. https://doi.org/10.1130/0091-7613(1997)025<0371:SAGDRT>2.3.CO;2

Gohl, K., Uenzelmann-Neben, G., Larter, R. D., Hillenbrand, C. D., Hochmuth, K., Kalberg, T., et al. (2013). Seismic stratigraphic record of the Amundsen Sea embayment shelf from pre-glacial to recent times: Evidence for a dynamic West Antarctic ice sheet. *Marine Geology*, *344*, 115–131. https://doi.org/10.1016/j.margeo.2013.06.011

Grunow, A. M., Kent, D. V., & Dalziel, I. W. D. (1991). New paleomagnetic data from Thurston Island: Implications for the tectonics of West Antarctica and Weddell Sea opening. *Journal of Geophysical Research*, *96*(B11), 17,935–17,954. https://doi.org/10.1029/91JB01507

Hart, S. R., Blijsztajn, J., & Craddock, C. (1995). Cenozoic volcanism in Antarctica: Jones Mountains and Peter I Island. *Geochimica et Cosmochimica Acta*, *59*(16), 3379–3388. https://doi.org/10.1016/0016-7037(95)00212-I

Holland, T., & Blundy, J. (1994). Non-ideal interactions in calcic amphiboles and their bearing on amphibole-plagioclase thermometry. *Contributions to Mineralogy and Petrology*, *116*(4), 433–447. https://doi.org/10.1007/BF00310910

Jarosewich, E., Nelen, J. A., & Norberg, J. A. (1980). Reference samples for electron microprobe analysis. *Geostandards Newsletter*, *4*(1), 43–47. https://doi.org/10.1111/j.1751-908X.1980.tb00273.x

Ketcham, R. A. (2005). Forward and inverse modeling of low-temperature thermochronometry data. *Reviews in Mineralogy and Geochemistry*, *58*(1), 275–314. https://doi.org/10.2138/rmg.2005.58.11

Ketcham, R. A., Carter, A., Donelick, R. A., Barbarand, J., & Hurford, A. J. (2007a). Improved modeling of fission-track annealing in apatite. *American Mineralogist*, *92*(5–6), 799–810. https://doi.org/10.2138/am.2007.2281

Ketcham, R. A., Carter, A., Donelick, R. A., Barbarand, J., & Hurford, A. J. (2007b). Improved measurement of fission-track annealing in apatite using *c*-axis projection. *American Mineralogist*, *92*(5–6), 789–798. https://doi.org/10.2138/am.2007.2280

Ketcham, R. A., Gautheron, C., & Tassan-Got, L. (2011). Accounting for long alpha-particle stopping distances in (U–Th–Sm)/He geochronology: Refinement of the baseline case. *Geochimica et Cosmochimica Acta*, *75*(24), 7779–7791. https://doi.org/10.1016/j.gca.2011.10.011

Kipf, A., Mortimer, N., Werner, R., Gohl, K., Van Den Bogaard, P., Hauff, F., & Hoernle, K. (2012). Granitoids and dykes of the Pine Island Bay region, West Antarctica. *Antarctic Science*, *24*(05), 473–484. https://doi.org/10.1017/S0954102012000259

Krohne, N., Lisker, F., Kleinschmidt, G., Klügel, A., Läufer, A., Estrada, S., & Spiegel, C. (2018). The Shackleton Range (East Antarctica): An alien block at the rim of Gondwana? *Geological Magazine*, *155*(04), 841–864. https://doi.org/10.1017/S0016756816001011

Larter, R. D., Cunningham, A. P., Barker, P. F., Gohl, K., & Nitsche, F. O. (2002). Tectonic evolution of the Pacific margin of Antarctica 1. Late Cretaceous tectonic reconstructions. *Journal of Geophysical Research*, *107*(B12), 2345. https://doi.org/10.1029/2000JB000052

Leat, P. T., Storey, B. C., & Pankhurst, R. J. (1993). Geochemistry of Palaeozoic–Mesozoic Pacific rim orogenic magmatism, Thurston Island area, West Antarctica. *Antarctic Science*, *5*(3), 281–296. https://doi.org/10.1017/S0954102093000380

LeMasurier, W. E. (2008). Neogene extension and basin deepening in the West Antarctic rift inferred from comparisons with the East African rift and other analogs. *Geology*, *36*(3), 247–250. https://doi.org/10.1130/G24363A.1

LeMasurier, W. E., & Landis, C. A. (1996). Mantle-plume activity recorded by low-relief erosion surfaces in West Antarctica and New Zealand. *Geological Society of America Bulletin*, *108*(11), 1450–1466. https://doi.org/10.1130/0016-7606(1996)108<1450:MPARBL>2.3.CO;2

LeMasurier, W. E., & Rocchi, S. (2005). Terrestrial record of post-Eocene climate history in Marie Byrd Land, West Antarctica. *Geografiska Annaler. Series A, Physical Geography*, *87*(1), 51–66. https://doi.org/10.1111/j.0435-3676.2005.00244.x

Lindow, J., Kamp, P. J., Mukasa, S. B., Kleber, M., Lisker, F., Gohl, K., et al. (2016). Exhumation history along the eastern Amundsen Sea coast, West Antarctica, revealed by low-temperature thermochronology. *Tectonics*, *35*, 2239–2257. https://doi.org/10.1002/2016TC004236

Lisker, F., & Läufer, A. L. (2013). The Mesozoic Victoria Basin: Vanished link between Antarctica and Australia. *Geology*, *41*(10), 1043–1046. https://doi.org/10.1130/G33409.1

Luyendyk, B. P. (1995). Hypothesis for Cretaceous rifting of east Gondwana caused by subducted slab capture. *Geology*, *23*(4), 373–376. https://doi.org/10.1130/0091-7613(1995)023<0373:HFCROE>2.3.CO;2

Luyendyk, B. P., Wilson, D. S., & Siddoway, C. S. (2003). Eastern margin of the Ross Sea Rift in western Marie Byrd Land, Antarctica: Crustal structure and tectonic development. *Geochemistry, Geophysics, Geosystems*, *4*(10), 1090. https://doi.org/10.1029/2002GC000462

McFadden, R. R., Teyssier, C., Siddoway, C. S., Cosca, M. A., & Fanning, C. M. (2015). Mid-Cretaceous oblique rifting of West Antarctica: Emplacement and rapid cooling of the Fosdick Mountains migmatite-cored gneiss dome. *Lithos*, *232*, 306–318. https://doi.org/10.1016/j.lithos.2015.07.005

Millar, I. L., Pankhurst, R. J., & Fanning, C. M. (2002). Basement chronology of the Antarctic Peninsula: Recurrent magmatism and anatexis in the Palaeozoic Gondwana Margin. *Journal of the Geological Society of London*, *159*(2), 145–157. https://doi.org/10.1144/0016-764901-020

Mortimer, N., Hoernle, K., Hauff, F., Palin, J. M., Dunlap, W. J., Werner, R., & Faure, K. (2006). New constraints on the age and evolution of the Wishbone Ridge, southwest Pacific Cretaceous microplates, and Zealandia–West Antarctica breakup. *Geology*, *34*(3), 185–188. https://doi.org/10.1130/G22168.1

Mortimer, N., Kohn, B., Seward, D., Spell, T., & Tulloch, A. (2016). Reconnaissance thermochronology of southern Zealandia. *Journal of the Geological Society*, *173*(2), 370–383. https://doi.org/10.1144/jgs2015-021

Mukasa, S. B., & Dalziel, I. W. (2000). Marie Byrd Land, West Antarctica: Evolution of Gondwana's Pacific margin constrained by zircon U-Pb geochronology and feldspar common-Pb isotopic compositions. *Geological Society of America Bulletin*, *112*(4), 611–627. https://doi.org/10.1130/0016-7606(2000)112<611:MBLWAE>2.0.CO;2

Müller, R. D., Gohl, K., Cande, S. C., Goncharov, A., & Golynsky, A. V. (2007). Eocene to Miocene geometry of the West Antarctic rift system. *Australian Journal of Earth Sciences*, *54*(8), 1033–1045. https://doi.org/10.1080/08120090701615691

Murray, K. E., Braun, J., & Reiners, P. W. (2018). Toward robust interpretation of low-temperature thermochronometers in magmatic terranes. *Geochemistry, Geophysics, Geosystems*, *19*, 3739–3763. https://doi.org/10.1029/2018GC007595

Mutch, E. J. F., Blundy, J. D., Tattitch, B. C., Cooper, F. J., & Brooker, R. A. (2016). An experimental study of amphibole stability in low-pressure granitic magmas and a revised Al-in-hornblende geobarometer. *Contributions to Mineralogy and Petrology*, *171*(10), 85. https://doi.org/10.1007/s00410-016-1298-9

Nelson, D. A., & Cottle, J. M. (2018). The secular development of accretionary orogens: Linking the Gondwana magmatic arc record of West Antarctica, Australia and South America. *Gondwana Research*, *63*, 15–33. https://doi.org/10.1016/J.GR.2018.06.002

Pankhurst, R. J., Millar, I. L., Grunow, A. M., & Storey, B. C. (1993). The pre-Cenozoic magmatic history of the Thurston Island crustal block, West Antarctica. *Journal of Geophysical Research*, *98*(B7), 11,835–11,849. https://doi.org/10.1029/93JB01157

Pankhurst, R. J., Weaver, S. D., Bradshaw, J. D., Storey, B. C., & Ireland, T. R. (1998). Geochronology and geochemistry of pre-Jurassic superterranes in Marie Byrd Land, Antarctica. *Journal of Geophysical Research*, *103*(B2), 2529–2547. https://doi.org/10.1029/97JB02605

Paolo, F. S., Fricker, H. A., & Padman, L. (2015). Volume loss from Antarctic ice shelves is accelerating. *Science*, *348*(6232), 327–331. https://doi.org/10.1126/science.aaa0940

Prenzel, J., Lisker, F., Balestrieri, M. L., Läufer, A., & Spiegel, C. (2013). The Eisenhower Range, Transantarctic Mountains: Evaluation of qualitative interpretation concepts of thermochronological data. *Chemical Geology*, *352*, 176–187. https://doi.org/10.1016/j.chemgeo.2013.06.005

Prenzel, J., Lisker, F., Elsner, M., Schöner, R., Balestrieri, M. L., Läufer, A. L., et al. (2014). Burial and exhumation of the Eisenhower Range, Transantarctic Mountains, based on thermochronological, sedimentary rock maturity and petrographic constraints. *Tectonophysics*, *630*, 113–130. https://doi.org/10.1016/j.tecto.2014.05.020

Prenzel, J., Lisker, F., Monsees, N., Balestrieri, M. L., Läufer, A., & Spiegel, C. (2018). Development and inversion of the Mesozoic Victoria Basin in the Terra Nova Bay (Transantarctic Mountains) derived from thermochronological data. *Gondwana Research*, *53*, 110–128. https://doi.org/10.1016/j.gr.2017.04.025

Pritchard, H., Ligtenberg, S. R. M., Fricker, H. A., Vaughan, D. G., Van den Broeke, M. R., & Padman, L. (2012). Antarctic ice-sheet loss driven by basal melting of ice shelves. *Nature*, *484*(7395), 502. https://doi.org/10.1038/nature10968–505.

Richard, S. M., Smith, C. H., Kimbrough, D. L., Fitzgerald, P. G., Luyendyk, B. P., & McWilliams, M. O. (1994). Cooling history of the northern Ford Ranges, Marie Byrd Land, West Antarctica. *Tectonics*, *13*(4), 837–857. https://doi.org/10.1029/93TC03322

Riley, T. R., Flowerdew, M. J., Pankhurst, R. J., Leat, P. T., Millar, I. L., Fanning, C. M., & Whitehouse, M. J. (2017). A revised geochronology of Thurston Island, West Antarctica, and correlations along the proto-Pacific margin of Gondwana. *Antarctic Science*, *29*(01), 47–60. https://doi.org/10.1017/S0954102016000341

Rocchi, S., LeMasurier, W. E., & Di Vincenzo, G. (2006). Oligocene to Holocene erosion and glacial history in Marie Byrd Land, West Antarctica, inferred from exhumation of the Dorrel Rock intrusive complex and from volcano morphologies. *Geological Society of America Bulletin*, *118*(7–8), 991–1005. https://doi.org/10.1130/B25675.1

Schmidt, M. W. (1992). Amphibole composition in tonalite as a function of pressure: An experimental calibration of the Al-in-hornblende barometer. *Contributions to Mineralogy and Petrology*, *110*(2–3), 304–310. https://doi.org/10.1007/BF00310745

Schwartz, J. J., Stowell, H. H., Klepeis, K. A., Tulloch, A. J., Kylander-Clark, A. R., Hacker, B. R., & Coble, M. A. (2016). Thermochronology of extensional orogenic collapse in the deep crust of Zealandia. *Geosphere*, *12*(3), 647–677. https://doi.org/10.1130/GES01232.1

Siddoway, C. S. (2008). Tectonics of the West Antarctic Rift System: New light on the history and dynamics of distributed intracontinental extension. In A. K. Cooper, P. J. Barrett, H. Stagg, B. Storey, E. Stump, W. Wise, & The 10th ISAES Editorial Team (Eds.), *Antarctica: A keystone in a changing world* (pp. 91–114). Washington, DC: National Academic Press. https://doi.org/10.3133/of2007-1047

Spiegel, C., Kohn, B., Belton, D., Berner, Z., & Gleadow, A. (2009). Apatite (U–Th–Sm)/He thermochronology of rapidly cooled samples: The effect of He implantation. *Earth and Planetary Science Letters*, *285*(1-2), 105–114. https://doi.org/10.1016/j.epsl.2009.05.045

Spiegel, C., Lindow, J., Kamp, P. J., Meisel, O., Mukasa, S., Lisker, F., et al. (2016). Tectonomorphic evolution of Marie Byrd Land—Implications for Cenozoic rifting activity and onset of West Antarctic glaciation. *Global and Planetary Change*, *145*, 98–115. https://doi.org/10.1016/j.gloplacha.2016.08.013

Storey, B. C., Brown, R. W., Carter, A., Doubleday, P. A., Hurford, A. J., Macdonald, D. I. M., & Nell, P. A. R. (1996). Fission-track evidence for the thermotectonic evolution of a Mesozoic–Cenozoic fore-arc, Antarctica. *Journal of the Geological Society*, *153*(1), 65–82. https://doi.org/10.1144/gsjgs.153.1.0065

Storey, B. C., Leat, P. T., Weaver, S. D., Pankhurst, R. J., Bradshaw, J. D., & Kelley, S. (1999). Mantle plumes and Antarctica-New Zealand rifting: Evidence from mid-Cretaceous mafic dykes. *Journal of the Geological Society*, *156*(4), 659–671. https://doi.org/10.1144/gsjgs.156.4.0659

Storey, B. C., Pankhurst, R. J., Millar, I. L., Dalziel, I. W. D., & Grunow, A. M. (1991). A new look at the geology of Thurston Island. In M. R. A. Thomson, J. A. Crame, & J. W. Thomson (Eds.), *Geological evolution of Antarctica. Proceedings of the Fifth International Symposium on Antarctic Earth Sciences* (pp. 399–403). Cambridge: Cambridge University Press.

Tulloch, A. J., Ramezani, J., Kimbrough, D. L., Faure, K., & Allibone, A. H. (2009). U-Pb geochronology of mid-Paleozoic plutonism in western New Zealand: Implications for S-type granite generation and growth of the east Gondwana margin. *Geological Society of America Bulletin*, *121*(9–10), 1236–1261. https://doi.org/10.1130/B26272.1

Vaughan, A. P., Leat, P. T., Dean, A. A., & Millar, I. L. (2012). Crustal thickening along the West Antarctic Gondwana margin during mid-Cretaceous deformation of the Triassic intra-oceanic Dyer Arc. *Lithos*, *142-143*, 130–147. https://doi.org/10.1016/j.lithos.2012.03.008

Veevers, J. J. (2012). Reconstructions before rifting and drifting reveal the geological connections between Antarctica and its conjugates in Gondwanaland. *Earth-Science Reviews*, *111*(3–4), 249–318. https://doi.org/10.1016/j.earscirev.2011.11.009

Wagner, G. A., Gleadow, A. J. W., & Fitzgerald, P. G. (1989). The significance of the partial annealing zone in apatite fission-track analysis: Projected track length measurements and uplift chronology of the Transantarctic Mountains. *Chemical Geology: Isotope Geoscience Section*, *79*(4), 295–305. https://doi.org/10.1016/0168-9622(89)90035-3

Weaver, S. D., Storey, B. C., Pankhurst, R. J., Mukasa, S. B., DiVenere, V. J., & Bradshaw, J. D. (1994). Antarctica-New Zealand rifting and Marie Byrd Land lithospheric magmatism linked to ridge subduction and mantle plume activity. *Geology*, *22*(9), 811–814. https://doi.org/10.1130/0091-7613(1994)022<0811:ANZRAM>2.3.CO;2

White, C. M., & Craddock, C. (1987). Compositions of igneous rocks in the Thurston Island area, Antarctica: Evidence for a late Paleozoic-middle Mesozoic Andinotype continental margin. *The Journal of Geology*, *95*(5), 699–709. https://doi.org/10.1086/629165

Wilson, D. S., Pollard, D., DeConto, R. M., Jamieson, S. S., & Luyendyk, B. P. (2013). Initiation of the West Antarctic Ice Sheet and estimates of total Antarctic ice volume in the earliest Oligocene. *Geophysical Research Letters*, *40*, 4305–4309. https://doi.org/10.1002/grl.50797

Wolf, R. A., Farley, K. A., & Kass, D. M. (1998). Modeling of the temperature sensitivity of the apatite (U–Th)/He thermochronometer. *Chemical Geology*, *148*(1–2), 105–114. https://doi.org/10.1016/S0009-2541(98)00024-2

Yakymchuk, C., Brown, C. R., Brown, M., Siddoway, C. S., Fanning, C. M., & Korhonen, F. J. (2015). Paleozoic evolution of western Marie Byrd Land, Antarctica. *Bulletin*, *127*(9–10), 1464–1484. https://doi.org/10.1130/B31136.1

Zachos, J., Pagani, M., Sloan, L., Thomas, E., & Billups, K. (2001). Trends, rhythms, and aberrations in global climate 65 Ma to present. *Science*, *292*(5517), 686–693. https://doi.org/10.1126/science.1059412

Zundel, M. (2018). Geodynamic evolution of the Pacific margin of West Antarctica based on apatite thermochronology (doctoral dissertation). Retrieved from library database (https://elib.suub.uni-bremen.de/edocs/00106584-1.pdf). University Bremen.

Erratum

In the originally published version of this article, in Table 1 a superscript keyed to footnote b was missing from the Ar-Ar column heading. In Table 2, there were several formatting errors in the column headings, and a column heading was missing from the third to last column. These errors have now been corrected, and this version may be considered the authoritative version of record.